Automated Detection and Forecasting of COVID-19 using Deep Learning Techniques: A Review

Afshin Shoeibi, Marjane Khodatars, Roohallah Alizadehsani, *Member, IEEE,* Navid Ghassemi, Mahboobeh Jafari, Parisa Moridian, Ali Khadem, Delaram Sadeghi, Sadiq Hussain, Assef Zare, Zahra Alizadeh Sani, Javad Bazeli and Fahime Khozeimeh, Abbas Khosravi, *Member, IEEE,* Saeid Nahavandi, *Fellow, IEEE,* U. Rajendra Acharya, *Senior Member, IEEE,* Peng Shi, *Fellow, IEEE*

Abstract—Coronavirus, or COVID-19, is a hazardous disease that has endangered the health of many people around the world by directly affecting the lungs. COVID-19 is a medium-sized, coated virus with a single-stranded RNA. This virus has one of the largest RNA genomes and is approximately 120 nm. The X-Ray and computed tomography (CT) imaging modalities are widely used to obtain a fast and accurate medical diagnosis. Identifying COVID-19 from these medical images is extremely challenging as it is time-consuming, demanding, and prone to human errors. Hence, artificial intelligence (AI) methodologies can be used to obtain consistent high performance. Among the AI methodologies, deep learning (DL) networks have gained much popularity compared to traditional machine learning (ML) methods. Unlike ML techniques, all stages of feature extraction, feature selection, and classification are accomplished automatically in DL models. In this paper, a complete survey of studies on the application of DL techniques for COVID-19 diagnostic and automated segmentation of lungs is discussed, concentrating on works that used X-Ray and CT images. Additionally, a review of papers on the forecasting of coronavirus prevalence in different parts of the world with DL techniques is presented. Lastly, the challenges faced in the automated detection of COVID-19 using DL techniques and directions for future research are discussed.

A. Shoeibi and N. Ghassemi are with the Faculty of Electrical Engineering, Biomedical Data Acquisition Lab (BDAL), K. N. Toosi University of Technology, Tehran, Iran, and the Computer Engineering Department, Ferdowsi University of Mashhad, Mashhad, Iran.

M. Khodatars and D. Sadeghi are with the Dept. of Medical Engineering, Mashhad Branch, Islamic Azad University, Mashhad, Iran.

R. Alizadehsani, A. Khosravi and S. Nahavandi. are with the Institute for Intelligent Systems Research and Innovation (IISRI), Deakin University, Victoria 3217, Australia. (Corresponding author: Abbas Khosravi, email: abbas.khosravi@deakin.edu.au).

M. Jafari is with Electrical and Computer Engineering Faculty, Semnan University, Semnan, Iran.

P. Moridian is with the Faculty of Engineering, Science and Research Branch, Islamic Azad University, Tehran, Iran.

A. Khadem is with the Faculty of Electrical Engineering, K. N. Toosi University of Technology, Tehran, Iran.

Sadiq Hussain is System Administrator at Dibrugarh University, Assam, India, 786004.

A. Zare is with Faculty of Electrical Engineering, Gonabad Branch, Islamic Azad University, Gonabad, Iran.

Z. Alizadeh Sani is with Rajaie Cardiovascular Medical and Research Center, and Iran University of Medical Sciences, Tehran, Iran.

F. Khozeimeh is with Faculty of Medicine, Mashhad University of Medical Sciences, Mashhad, Iran.

U. R. Acharya is with the Dept. of Electronics and Computer Engineering, Ngee Ann Polytechnic, Singapore 599489, Singapore, the Dept. of Biomedical Informatics and Medical Engineering, Asia University, Taichung, Taiwan, and the Dept. of Biomedical Engineering, School of Science and Technology, Singapore University of Social Sciences, Singapore.

P. Shi is with the School of Electrical and Electronic Engineering, University of Adelaide, Adelaide, SA 5005, Australia.

Index Terms—COVID-19, Diagnosis, Deep Learning, Classification, Segmentation, Forecasting.

I. INTRODUCTION

The novel COVID-19 virus came to light in December 2019 in Wuhan Province, China, where it originated from animals and quickly spread around the world [1]. The easiest way to transmit COVID-19 is through the air and physical contact, such as hand contact with an infected person [2]. The virus inserts itself into the lung cells through the respiratory system and replicates there, destroying these cells [3]. COVID-19 comprises an RNA and is very difficult to diagnose and treat due to its mutation characteristics [4]. The most common symptoms of COVID-19 include fever, cough, and shortness of breath, dizziness, headache, and muscle aches [5]. The virus is so perilous and can provoke the death of people with weakened immune systems [6]. Infectious disease specialists and physicians around the world are working to discover a treatment for the disease. COVID-19 is currently the leading cause of death for thousands of countries worldwide, including the USA, Spain, Italy, China, the United Kingdom, Iran, and others. Figure 1 exhibits the latest number of infected people worldwide due to COVID-19.

The detection of COVID-19 is crucially significant and vital in its early stages. Various methods have been proposed to diagnose COVID-19, containing a variety of medical imaging techniques, blood tests (CBCs), and PCR. According to the WHO, all diagnoses of corona disease must be confirmed by reverse-transcription polymerase chain reaction (RT-PCR) [7]. However, testing with RT-PCR is highly time-consuming, and this issue is risky for people with COVID-19. Hence, first, medical imaging is carried out for the primary detection of COVID-19, then the RT-PCR test is performed to aid the physicians in making final accurate detection. Two medical imaging techniques, X-ray and CT-scan, are employed to diagnose COVID-19 [8], [9].

X-ray modality is the first procedure to diagnose COVID-19, which has the advantage of being inexpensive and low-risk from radiation hazards to human health [10], [11]. In the X-ray method, detecting COVID-19 is a relatively complicated task. In these images, the radiologist must attentively recognize the white spots that contain water and pus, which is very prolonged and problematic. A radiologist or specialist doctor may also mistakenly diagnose other diseases, such as pulmonary tuberculosis, as COVID-19 [12].
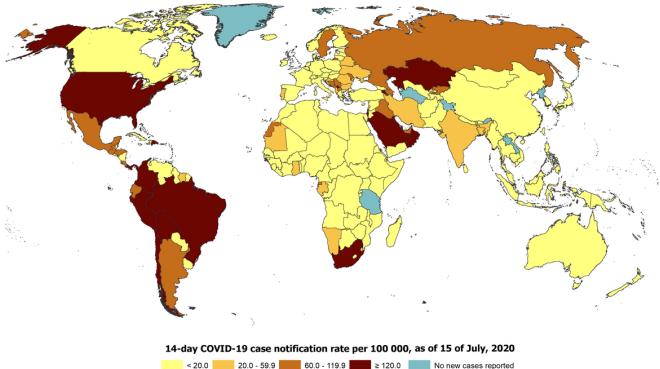
Fig. 1: Detailed statistics of COVID-19 infected people world-wide [13].

Fig. 2: Number of papers published on COVID-19 using DL techniques.

The X-ray procedure has a high error rate; hence CT images can be used for more precise detection [14]. Nevertheless, these CT images are far more expensive than X-rays for patients [15]. At the time of CT-scan recording, several slices are provided from each person suspected of COVID-19. The large volume of CT-Scan images calls for a high workload on physicians and radiologists to diagnose COVID-19.

In recent years, applications of artificial intelligence in medicine have led to a variety of studies aiming to diagnose varied diseases, including brain tumors from MR images [16], [17], multiple types of brain disorders such from EEG [18], [19], breast cancer from mammographic images [20], [21] and pulmonary diseases such as Covid-19 from X-Ray [22] and CT-Scan [23]. In the last decade, Deep Learning (DL), a branch of machine learning, has changed the expectations in many applications of artificial intelligence in data processing by reaching human-level accuracies [24] in many tasks, including medical image analysis [25].

In this paper, an overview of COVID-19 diagnostic approaches utilizing DL networks is presented. Section II explains the search strategy, and various DL models developed for COVID-19 detection are described in Section III. Section IV of the DL techniques used for the detection, segmentation, and prediction of COVID-19 patients. Section V discusses the reviewed papers on diagnosis, segmentation, and prediction of COVID-19 patients. Challenges in diagnosing, segmentation, and prediction of COVID-19 patients are provided in Section VI. Finally, the summary and future work are delineated in Section VII.

II. SEARCH STRATEGY

In this study, valid databases, including IEEE Xplore, ScienceDirect, SpringerLink, ACM, and ArXiv, have been used to search for Covid-19 papers. Moreover, a more detailed Google Scholar search is employed. The articles are selected using the keywords COVID-19, Corona Virus, Deep Learning, Segmentation, and Forecasting. The latest selection of papers is done with the mentioned keywords on July 11th, 2020. Figure 2 indicates the number of papers published or indexed by COVID-19 using DL techniques using various databases.
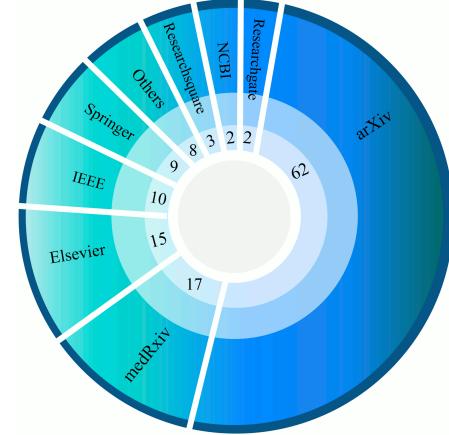
III. DEEP LEARNING TECHNIQUES FOR COVID-19 DETECTION

Traditional machine learning and DL are the two significant branches of AI, but DL is essentially a more advanced version of traditional machine learning (ML). Various DL networks have been extensively used to diagnose the COVID-19 accurately using many public databases.

DL architectures, namely convolutional neural networks (CNNs), recurrent neural networks (RNNs), Autoencoders (AEs), deep belief networks (DBNs), generative adversarial networks (GANs), and hybrid networks such as CNN-RNN and CNN-AE have been developed for automated detection of COVID-19. Figure 3 exhibits the subcategories of DL networks.

IV. COMPUTER AIDED DIAGNOSIS SYSTEM (CADS) FOR COVID-19 DETECTION

Many CADS have been developed using DL methods using X-ray and CT images. Two types of systems: (i) classification and (ii) segmentation using DL methods have been developed. In classification-based CADS, the main objective is to identify COVID-19 patients, which involves the process of extracting features, selecting features, and classifying using deep layers. The second type, CAD, is for the segmentation of X-Ray and CT-Scan images of each infected person with COVID-19. Segmentation implies dividing images into meaningful areas and is of particular notability in medicine. Manual segmentation of medical images takes much time; thus, applying machine learning models is crucially paramount. Among the most important segmentation models, the various types of fuzzy clustering methods [26], [27] and DL procedures such as U-Net [28] can be expressed. In the CADS, with the segmentation approach, patients' CT-Scan images and their manual segments labeled by doctors are fed to the DL network. Then, during the training process, the DL network is trained on manual segments to segment raw input images. Finally, in deep network output, segmented images are presented with segmentation accuracy. The components of DL-based CADS for COVID-19 detection are shown in Figure 4. In
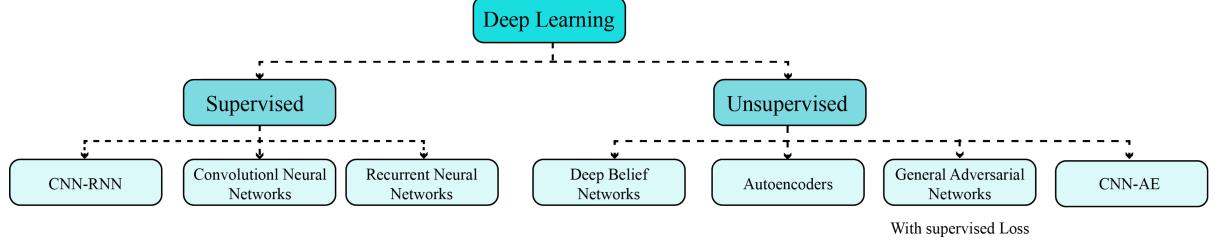
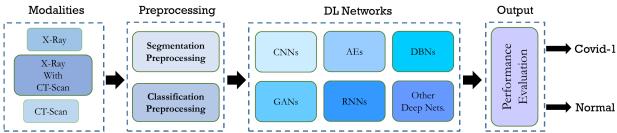Fig. 3: Illustration of various DL methods used for COVID-19 detection.

Fig. 4: Block diagram for COVID-19 detection using DL technique.

TABLE I: Public databases used for COVID-19 detection.

Dataset	Modality	Link
J. P. Cohens GitHub [29]	X-ray and CT	https://github.com/ieee8023/covid-chestxray-dataset
European Society of Radiology	X-ray and CT	https://www.eurorad.org/advanced-search?search=COVID
SIRM	X-ray and CT	https://www.sirm.org/category/senza-categoria/covid-19
BSTI	X-ray and CT	https://www.bsti.org.uk/covid-19-resources
UCSD-AI4H [30]	CT	https://github.com/UCSD-AI4H/COVID-CT
MedSeg	CT	http://medicalsegmentation.com/covid19
Kaggle	X-ray and CT	https://www.kaggle.com/datasets?search=covid
Point-of-Care Ultrasound (POCUS) [31]	Lung Ultrasound Images and Videos	https://github.com/jannisborn/covid19_pocus_ultrasound
Actualmed COVID-19 Chest X-ray Dataset Initiative	X-ray	https://github.com/agchung/Actualmed-COVID-chestxray-dataset
COVID-19 Chest X-ray Dataset Initiative	X-ray	https://github.com/agchung/Figure1-COVID-chestxray-dataset
Georgia State Universitys Panacea Lab [32]	Twitter Chatter Dataset	https://github.com/thepanacealab/covid19_twitter
Twitter COVID19 CXR dataset	X-ray	https://twitter.com/ChestImaging
COVID-19 [33]	CT	https://github.com/KevinHuRunWen/COVID-19
COVIDx [34]	X-ray	https://github.com/lindawangg/COVID-Net

TABLE II: Public COVID-19 forecasting databases used for forecasting.

Dataset	Modality	Link
China CDC Weekly	Daily Number of Cases in China	http://weekly.chinacdc.cn/news/TrackingtheEpidemic.htm
The Ministry of Health and Family Welfare (Government of India)	Daily Number of Cases in India	https://www.mohfw.gov.in
Johns Hopkins University	Tracking COVID-19 Spread	https://systems.jhu.edu
WHO COVID-19 Dashboard	Global Statistics	https://covid19.who.int
U.S. CDC	Daily Number of Cases in U.S.	https://www.cdc.gov/coronavirus/2019-ncov/cases-updates/cases-in-us.html https://www.cdc.gov/coronavirus/2019-ncov/covid-data/data-visualization.htm
Worldometer	Global Collection	https://www.worldometers.info/coronavirus
Open Source COVID-19	Global Collection	http://open-source-covid-19.weileizeng.com
Painel Coronavírus	Daily Number of Cases in Brazil	https://covid.saude.gov.br
GOV.UK	Daily Number of Cases in UK	https://coronavirus.data.gov.uk
Ministero della Salute	Daily Number of Cases in Italy	http://www.salute.gov.it/portale/nuovocoronavirus/homeNuovoCoronavirus.jsp?lingua=english
Ministry of health	Daily Number of Cases in Spain	https://www.mscbs.gob.es/profesionales/saludPublica/ccayes/alertasActual/nCov-China/situacionActual.htm https://cnecovid.isciii.es/covid19
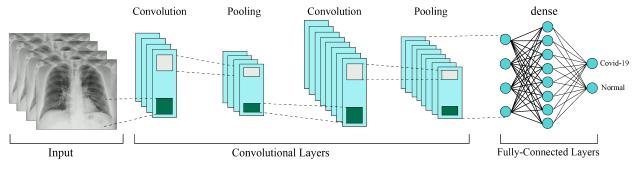
Fig. 5: Typical 2D-CNN architecture used for COVID-19 detection.

the following section, we will first mention the important data available for COVID-19. Then, the DL methods exploited in the research are introduced.

A. Public Databases used for COVID-19 Detection and Forecasting

Various public databases (X-ray and CT images) available for the detection and prediction of COVID-19 are listed in Table I. Also, the databases used to predict the corona spread in leading countries of the world are shown in Table II.

B. Deep Learning Methods

DL networks developed for classification, segmentation, and prediction of COVID-19 disease will be analyzed in this section. Various applied DL architectures are discussed briefly in the following sections.

1) Classification Models: Various DL methods presented for the automated detection of COVID-19 are discussed in this section. 2D CNN, AlexNet, Visual Geometry Group (VGG) network, GoogLeNet, DenseNet, XceptionNet, MobileNet, SqueezeNet, Inception-ResNet, CapsNet, NasNet-mobile, ShuffleNet, EfficientNet, and Generative Adversarial Networks (GAN) have been used for the automated detection of COVID-19 patients using X-ray and CT images.

STANDARD 2D-CNN

The primary issue in training the deep models is the concern of overfitting that occurs from the gap between the limited number of training samples and a large number of learnable parameters. Convolutional networks try to overcome this by using convolutional layers. CNNs require minimal pre-processing by considering the 2-dimensional (2D) images as input, and hence it is designed to retain and utilize the structural information among neighboring pixels or voxels. A differentiable function is utilized to transform one volume of actions by each layer to the other as it is a sequence of layers structurally. Figure 6 represents the architecture for a usual computer vision job that comprises of three neural layers: convolutional, pooling, and fully connected layers. The convolutional layers are usually combined with the pooling layers, and their output is fed to the fully connected layers [35]. Also, a variety of methods like dropout and batch normalization help these networks to learn better [35].

ALEXNET

As the first famous deep learning network, Alexnet is still the center of attention in many studies. Figure 6 depicts the architecture of AlexNet. In this network, two new perspectives dropout, and local response normalization (LRN) are used to help the network learn better. Dropout is applied in two FC layers employed in the end. On the other hand, LRN,
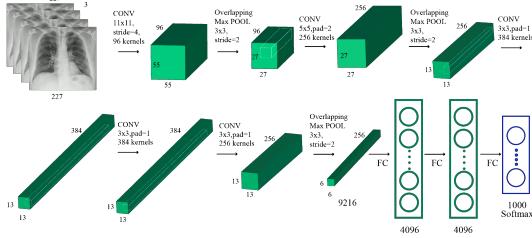
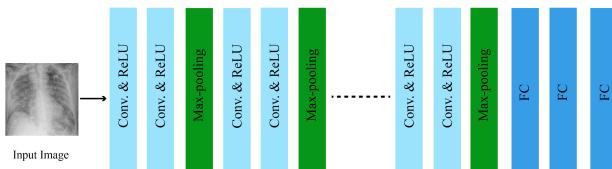Fig. 6: A typical AlexNet architecture used for COVID-19 detection.

Fig. 7: A typical VGG architecture used for COVID-19 detection.

Fig. 8: Naive version of inception layer.

Fig. 9: Inception layer with dimension reduction.

utilized in convolutional layers, can be employed in two different ways: Firstly, applying single channel or feature maps, where the same feature map normalizes depending on the neighborhood values and selects the NN patch. Secondly, LRN can be exploited across the channels or feature maps [36], [37].

VGGNET

The VGG architecture comprised of a few convolutional layers, each of that utilizes the ReLU activation function. For classification, this network uses a softmax classifier in the final layer of the model. Filter size for convolutional layers is picked equal to 3x3, with a stride of 2 in VGG-E. VGG-11, VGG-16, and VGG-19 are three variants of the VGG-E model that have 11, 16, and 19 layers correspondingly. All variants of VGG-E architecture end with three FC layers. Nevertheless, the numbers of convolution layers are different; VGG-19 contains 16 convolution layers, VGG-16 has 13 convolution layers, and VGG-11 has eight convolution layers. Figure 7 depicts the building block of the VGG network used for COVID-19 detection [36], [38].

GOOGLENET

Different receptive fields, generated by various kernel sizes, form Inception layers, which are incorporated in this model. Operations generated by these receptive fields records sparse correlation patterns in the novel feature map stack [36]. Figure 8 describes the initial concept of the inception layer. A stack of inception layers is utilized by GoogLeNet to enhance recognition accuracy, as shown in Figure 9. The difference between the final inception layer and the nave inception layer is the inclusion of 1x1 convolution kernels, which performs a dimensionality reduction, consequently reducing the computational cost. Another idea in GooGLeNet is the gradient 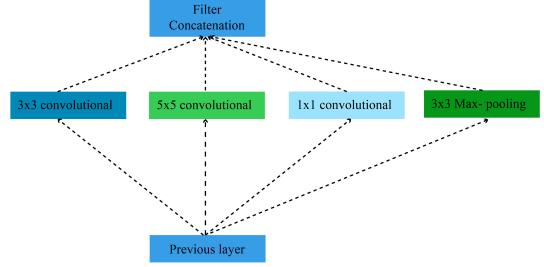injec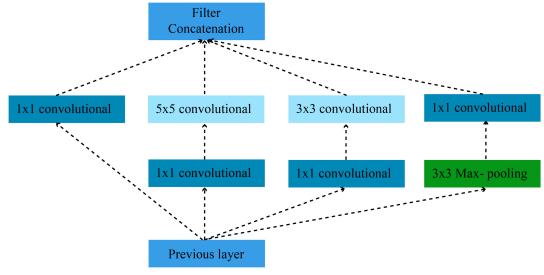tion, which aims to overcome the gradient vanishing problem. GoogLeNet comprises of a total of 22 layers that is greater than any previous network. However, GoogLeNet uses much fewer parameters compared to its predecessors VGG or AlexNet [36], [39].

RESNET

The Residual Network (ResNet) is created with various numbers of layers; 1202,152, 101, 50, and 34. ResNet50 is one of the popular variants containing 49 convolution layers and 1 FC layer at the end of it. The total number of MACs and weights are 3.9M and 25.5M, respectively [36], [40], [41]. Figure 10 shows a typical ResNet architecture used for COVID-19 detection.

DENSENET

The DenseNet that comprised of densely connected CNN layers, in a dense block [36], [43] with the outputs of each layer are connected with all descendant layers. Due to the dense connectivity between the layers, it is termed as DenseNet. Network parameters are reduced dramatically by efficient utilization of feature reuse. DenseNet comprises of various transition blocks and dense blocks that are situated in between two adjacent dense blocks. Figure 11 describes the conceptual diagram of a dense block [36].

XCEPTIONNET

The Xception architecture is based on Inception V3. The Xception architecture is a linear stack of depth-wise separable convolution layers with residual connections. The network entails 36 layers of convolution organized in 14 modules, all of which contain linear residual connections around them, except for the first and last modules. Utilizing residual connections in Xception architecture will lead to faster convergence and superior final performance [44].

MOBILENET

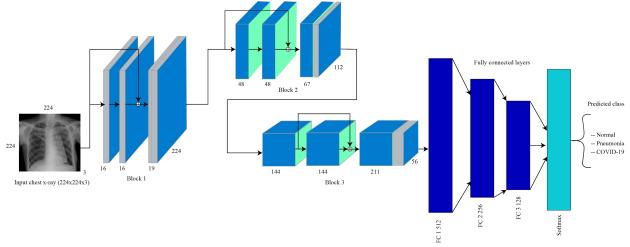The novel model called MobileNets is aimed to be used

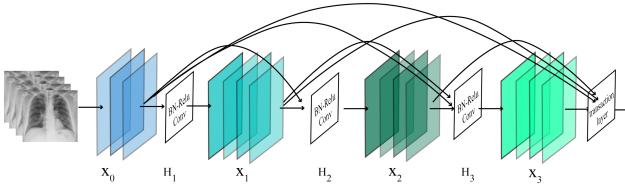Fig. 10: A typical ResNet architecture used for COVID-19 detection [42].

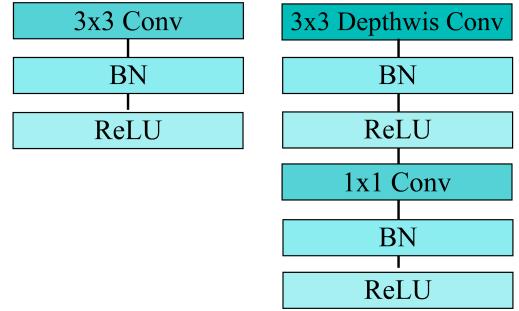Fig. 11: A 4-layer dense block with growth rate of k=3 used for COVID-19 detection [36].

Fig. 12: Left: standard CNN layer with BN and ReLU. Right: Depth-wise separable convolutions with depth-wise and Point-wise layers followed by BN and ReLU.

in mobile and embedded machine vision applications [45]. The main layers exploited in this architecture are known as depthwise separable convolution. The depthwise separable convolution consists of two layers: depthwise convolution, and pointwise convolution. The depthwise convolution is used to apply a single filter to each input channel (input depth). Then the pointwise convolution, simple 1x1 convolution, is employed to create a linear combination of depthwise layer outputs. After both of these layers, a ReLU and batch normalization (BN) are placed (Figure 12) [46].

SQUEEZENET

Using three architectural design strategies, this structure has introduced a fire module [47]. The module consists of a squeeze-convolution layer that has only 1x1 filters, followed by an expansion layer that has a set of 1x1 and 3x3 convolution filters. With slight modification and optimization in the original SqueezeNet architecture, two other architectures, SqueezeNet with simple bypass and SqueezeNet with complex bypass, were also demonstrated. By benchmarking the SqueezeNet architecture on the ImageNet database and comparing its results with the AlexNet architecture, it was found that the SqueezeNet accuracy is at the AlexNet level, but the 50X has a lower parameter, and the model size is less than 0.5MB [47].

INCEPTION-RESNET

In 2016, Szegedy et al. proposed the idea of integrating Inception architecture with residual connections, meaning that the filter concatenation stage in Inception architecture would be replaced by residual connections [41]. The idea led to a new architecture called Inception-ResNet, which has two versions, V1 and V2. At the same time, another architecture named Inception V4 was introduced, in which reduction blocks were exploited. These blocks are modified versions of Inception

modules. Finally, it was perceived that introducing residual connections to Inception architecture significantly improves training speed. Also, both of these architectures have outperformed than previous architects [41].

CAPSNET

With advancements of CNNs and new structures, they have reached high accuracies on many tasks. However, one of the deficiencies of CNN models is when they face samples drown from a dataset with a different orientation than a training dataset. To address this, CapsNet was proposed. The central idea behind this network is to create a network that implicitly performs an operation similar to inverse graphics; i.e., it tries to find graphical shapes in an image. The building block of this structure is capsules, which try to determine whether an object is presented at a given location and find its instantiation. With the help of these capsules, CapsNet performs better than its prior models in many tasks and specifically in cases where two classes have a considerable overlap [48].

NASNET-MOBILE

In a try to find a method to learn architecture directly from data instead of handly designing it [49], NASNet was created. First, the best normal convolution cell and the reduction convolution cell are found in NASNet's search space by applying the RNN controller, on a small dataset. The RNN controller then stacks multiple copies of these cells with various parameters to acquire NASNet architecture. A new regularization technique called ScheduledDropPath has also been stated, which dramatically meliorate the generalizability of NASNet models. The architectures obtained on the COCO object detection database have also been evaluated in all cases, showing that the architectures could achieve state-of-the-art performance [49].

SHUFFLENET

ShuffleNet is specially designed for mobile devices with minimal computing power [50], [51]. This architecture employs two operations, pointwise group convolution and channel shuffle, to maintain the network's accuracy while reducing the computational cost. ShuffleNet architecture embraces a convolution layer, two pooling layers, a stack of ShuffleNet units that are structured in three stages, and finally, an FC layer. Although ShuffleNet is designed for small models, it still
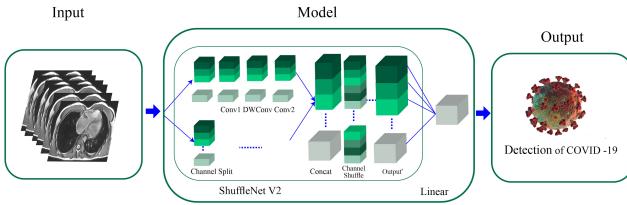
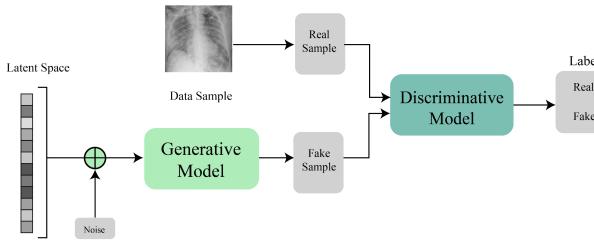Fig. 13: A typical ShuffleNet for COVID-19 detection [52].

Fig. 14: A Simple GAN architecture.

surpasses MobileNet (lower computation cost, higher training speed). Figure 13 shows a general form of ShuffleNet used for COVID-19 detection.

EFFICIENTNET

The fundamental building block in EfficientNet was to overcome the MBConv mobile bottleneck. The EfficientNet architecture developed using the compound scaling method, which led to the EfficientNet-B0 to B7. It is found that this architecture has fewer parameters of 8.4x and a faster running time of 6.1x [53].

2) Generative Adversarial Networks (GAN): A primary problem in training deep models is limits in dataset size. Using generative models for data augmentation is one solution to this issue. Due to the high quality of generated data, GANs have attracted attention in the medical imaging community [54]. The basic idea in training a GAN is a simple minimax game, in which one network tries to distinguish between real data and generates one, and the other tries to create data undistinguishable by the first network [55], therefor creating images similar to real data. Figure 14 shows a simple gan architecture.

3) Segmentation Models: In this section, various DL models developed to segment the lung region to detect the COVID-19 patients accurately are discussed. FCN network, SegNet, U-Net, and Res2Net DL models are widely used for the segmentation of lungs and are briefly discussed below.

FULLY CONVOLUTIONAL NETWORK (FCN)

In this model, popular networks have transformed entirely convolutional models by replacing FC layers with convolution layers to capture output as a local map. These maps are up-sampled using the introduced method, which uses a backward convolution with stride size f, capable of learning. At the end of the network, there is a 1x1 convolution layer that yields the corresponding pixel label as the output. The exiting stride in
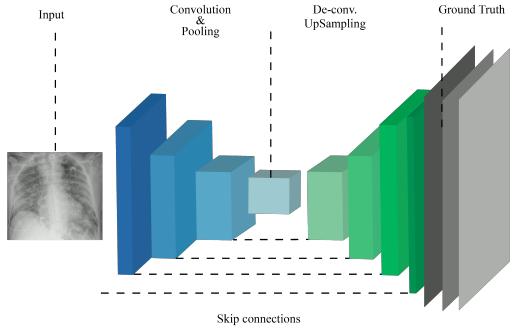
Fig. 15: A typical FCN architecture used for segmentation of lung in COVID-19 patients.
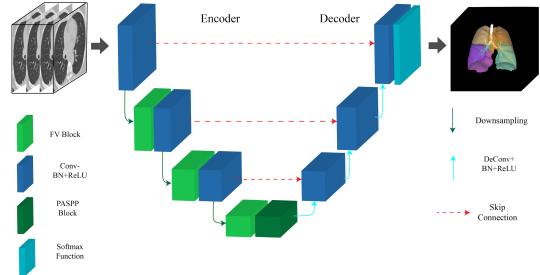
Fig. 16: A typical SegNet architecture used to segment lung in COVID-19 patients [58].

the deconvolution stage constraints the output detail quantity of this layer. To address this issue and enhance the quality of the result, several skip connections have been added to the network from the lower layers to the end layer [56]. Figure 15 shows a general form of FCN used for the segmentation of lung in COVID-19 patients.

SEGNET

Generally, in segmentation techniques, a network created for classification is chosen, and the FC layers of that network are removed; the resulting network is called the encoder network. Then a decoder is created to transform these low-resolution maps to the original resolution. In SegNet [57], the decoder is created such that for each down-sampling layer in the encoding section, an up-sampling layer is positioned in the decoder. These layers, unlike the deconvolution layers of FCN networks, are not capable of learning, and the values are placed at the locations from which the corresponding max-pooling layer is extracted, and the rest of the output cells become zero. Figure 16 shows a general form of SegNet used for the segmentation of lung in COVID-19patients.

U-NET

The U-Net network [59], like SegNet, consists of the identical numbers of pooling and up-sampling layers, but the network utilizes trainable deconvolution layers. Also, in this network, there is a corresponding skip connection between the up-sampling and down-sampling layers. Figure 17 shows

Fig. 17: A typical U-Net architecture used to segment the lung in COVID-19 patients [60].

(a) Long Short-Term Memory   (b) Gated Recurrent Unit

Fig. 18: Architecture of LSTM (a) and GRU (b). In the figure a, the yellow, green and blue represent output gate, input gate and forget gate respectively. In the figure b, the yellow and blue represent the update and reset gate respectively. Biases are not shown to keep the figure simple [35].

a general form of U-Net architecture used to segment the lung in COVID-19 patients.
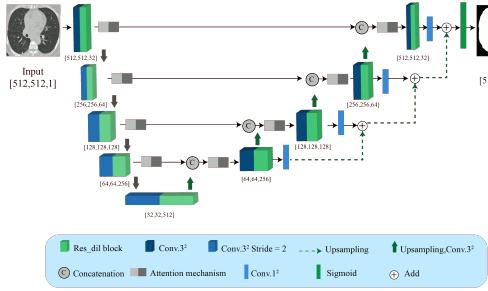
RES2NET

In the Res2Net module, after the 1*1 convolution, the feature maps are divided into several subsets, then passed through a set of 3*3 filters. Their outputs are concatenated together and then go through the 1*1 convolution [61]. The set of this process is residually structured. For that reason, it is named as Res2Net module. This module introduces a new control parameter called the scale dimension (the number of feature groups in the Res2Net block); with an increase of scale, features with richer receptive field sizes are learned by the model. The Res2Net module is capable of integrating with modern modules such as cardinality dimension and squeeze and excitation (SE). It can also be integrated easily with state-of-the-art models, such as ResNet, ResNeXt, DLA, Big-Little Net, which are called Res2Net, Res2NeXt, Res2Net-DLA, and bLRes2Net-50, respectively [61].

4) Forecasting Models: RECURRENT NEURAL NETWORK(RNN)

A feed-forward neural network is extended to create RNN, aiming to capture the long term dependencies and features from the sequential and time-series data. The most commonly used RNN is the long-short term memory (LSTM), which composed of a memory cell C_t, a forget cell f_t, the input gate i_t, and output gate o_t (figure 18(a)). These gates make the decision that which information needs to be remembered or discarded from the memory cell and also organizes the activation signals from different sources.

LSTM decides whether to keep or remove the memory by using these gates, unlike vanilla RNN, LSTM can preserve the potential long term dependencies of a feature, which is learned from the input sequential data. One LSTM variant is Gated Recurrent Unit (GRU) [62], which integrates the forget and input gates into a single update gate and combines the memory cell state and the hidden state into one state (figure 18(b)). Update gate makes a decision on the amount of information to be added or discarded, and the reset gate decides on how much earlier information is to be forgotten. This technique makes GRU simpler than LSTM.

AUTOENCODERS (AES)
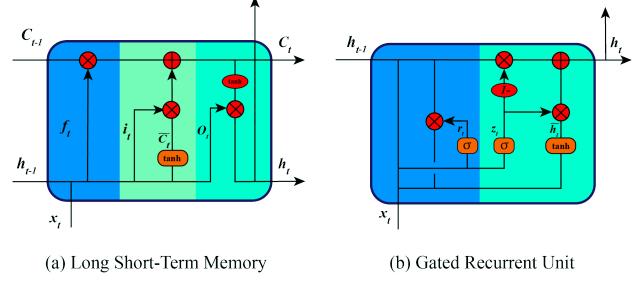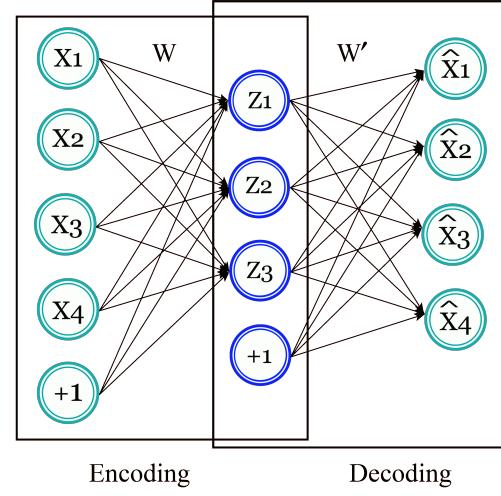
Fig. 19: Diagram of Autoencoder.

Autoencoder (AE) is a neural network method with competent data encoding and decoding strategies used for unsupervised feature learning [35]. The primary purpose of AE is usually to learn and representation of data (encoding), as well as dimensionality reduction of data, fusion, compression, and many more [63], [64]. The AE models comprised of two phases: encoder and decoder. The input samples are mapped typically to a lower-dimensional space with beneficial feature representation in the encoding part. Reverse processing is applied in the decoding phase to revert data to its original space, trying to create data from lower space representation. Figure 19 depicts the conceptual diagram of AE with encoding and decoding phases.

TABLE III: Summary of state-of-art DL techniques used for the automated detection of COVID-19 patients.

Work	Dataset	Modalities	Number of Cases	Preprocessing	DNN toolbox	DNN	Number of Layers	Classifier	Post Processing	K-Fold	Performance Criteria (%)
[65]	COVIDx	X-ray	45 COVID-19, 1203 Normal, 931 Bacterial Pneumonia, 660 Viral Pneumonia Patients	Data Augmentation (DA), Rescaling, Normalizing	Fastai Library	COVID-ResNet (ResNet-50)	Modified Version	Softmax	NA	NA	Acc=96.23 Sen=100 Pre=100 F1-Score=100
[66]	Combination of Different Datasets	X-ray	50 COVID-19, 50 Normal Images	Rescaling	NA	ResNet50	Modified Version	Softmax	NA	5	Acc=98 Recall=96 Spe=100
[67]	Combination of Different Datasets	X-ray, CT-Scan	85 COVID-19 X-ray, 203 COVID-19 CT-scan, 85 Normal X-ray, 153 Normal CT-scan	Cropping, resizing	NA	AlexNet	Modified Version	Softmax	NA	NA	Acc=98 Sen=100 Spe=96
[68]	Cohens GitHub	X-ray	25 COVID-19, 25 Normal Cases	Rescaling	Keras with Tensor-Flow2 Backend	COVIDX-Net (VGG19, DenseNet201)	Standard Version	Softmax	NA	NA	Acc=90 Pre=83 F1-Score=91
[69]	Combination of Different Datasets	X-ray	70 COVID-19 subjects, 1008 Pneumonia Subjects	Rescaling, DA	NA	ResNet-18	Standard Version + 8	Sigmoid	Grad-CAM	NA	Sen=96 Spe=70.65 AUC=95.18
[70]	COVIDx	X-ray	266 COVID-19 Patient Cases, 8,066 Normal Patient Cases, 5,538 Non-COVID19 Pneumonia Patient Cases	DA	Keras with Tensor-Flow Backend	COVID-Net	87	Softmax	Explainability-Driven Audit (GSInquire Method)	NA	Acc=93.3 Sen=91 PPV=98.9
[71]	COVIDx	X-ray	76 COVID-19, 1583 Normal, 4290 Pneumonia Cases	DA, RGB format, Normalizing	MATLAB	COVIDiagnosis-Net	Standard Version	Decision-Making System	Class Activation Mapping Visualization	NA	Acc=98.3 Spe=99.13 F1-Score=98.3
[72]	Combination of Different Datasets	X-ray	68 COVID-19, 1583 Normal, 2786 Bacterial Pneumonia, 1504 Viral Pneumonia Images	Resizing, Standardizing, DA	Keras	ResNet50-V2	Modified Version	Softmax	saliency Maps Visualization, Different Gradient Methods	NA	Predictive Entropy=99.68 BALD=88.73
[73]	Combination of Different Datasets	X-ray	295 COVID-19, 65 Normal, 98 Pneumonia Images	Fuzzy Color Method, Image Stacking Technique	MATLAB	MobileNetV2 SqueezeNet	Standard Version	SMO, SVM	Social Mimic Optimization Method	5	Acc=99.27
[74]	Clinical	CT-Scan	368 COVID-19 Patients, 127 Patients with Other Pneumonia	Segmentation, Rescaling, Multi-view Fusion	Keras	ResNet50	Modified Version	Dense Layer	NA	NA	Acc=76 Sen=81.1 Spe=61.5
[75]	Combination of Different Datasets	X-ray	127 COVID-19, 500 No-Findings and 500 Pneumonia Images	NA	NA	DarkCovidNet (CNN)	39	Linear	Interpretation of Heatmaps Results of the DarkCovidNet Model by an Expert Radiologist	5	2-classes: Acc=98.08 Spe=95.3 Sen=95.13 Pre=98.03 F1-Score=96.51 3 classes: Acc=87.02 Spe=92.18 Sen=85.35 Pre=89.96 F1-Score=87.37
[76]	Clinical	CT-Scan	108 COVID-19, 86 Non-COVID-19 Patients	Different Methods	NA	ResNet-101, Xception	Standard Version	Softmax	NA	NA	Sen=98.04 Spe=100 Acc=99.02
[77]	Combination of Different Datasets	X-ray	105 COVID-19 ,11 SARS, 80 Normal Samples	DA, Histogram, Feature Extraction using AlexNet, PCA, K-means	MATLAB	DeTraC (ResNet18)	Standard Version	Softmax	Composition Phase	NA	Acc=95.12 Sen=97.91 Spe=91.87
[78]	RYDLS-20	X-ray	90 COVID-19, 10 MERS, 11 SARS, 10 Varicella, 12 Streptococcus, 11 Pneumocystis Samples	Different Features, Early Fusion, Late Fusion, Different Resampling Algorithms	NA	Inception-V3	Standard Version	MLP / Clus-HMC Framework	Friedman Statistical Test for Ranking	NA	F1-Score=83.33 / F1-Score=88.89
[79]	Pneumonia Dataset	X-ray	624 Images in 2 Categories: Normal and Pneumonia	GAN	MATLAB	ResNet18	Standard Version	Softmax	NA	NA	Acc=99 Pre=98.97 F1-Score=98.97
[80]	SIRM Dataset	CT-Scan	53 Infected CT Images	Two Different Patch Datasets	NA	VGG-16, GoogleNet and ResNet-50 (Feature Extraction)	Standard Version	SVM	NA	NA	Acc=98.27 Sen=98.93 Spe=97.60 Pre=97.63 F1-Score=98.28
[81]	COVIDx	X-ray	NA	NA	NA	COVID-CAPS	9	Capsule Layer	NA	NA	Acc=95.7 Sen=90 Spe=95.8
[82]	Combination of Different Datasets	X-ray	284 Covid-19, 310 Normal, 330 Pneumonia Bacterial, 327 Pneumonia Viral Images	Rescaling	Keras with Tensor-Flow Backend	CoroNet	Modified Version	Softmax	NA	NA	Acc=89.5 Pre=97 F1-Score=98
[83]	Kaggle	X-ray	5,863 X-Ray Images in Two Classes Normal and Pneumonia, 145 Chest X-ray Images of COVID-19	Rescaling	Keras with Tensor-Flow Backend	DenseNet169	Standard Version	Softmax	NA	NA	Avg Acc=95.72
[84]	COVIDx	X-ray	13; 800 Images from 13; 645 Individuals	Intensity Normalization, DA	Keras with Tensor-Flow Backend	EfficientNet B3	50	Softmax	Activation Map Visualization	NA	Acc=93.9 Sen=96.8
[42]	3 Different COVIDx Datasets	X-ray	Different Number of Cases	Different Methods	Keras with Tensor-Flow Backend	DenseNet-161	Modified Version	Softmax	Grad-CAM, Grad-CAM++, LRP Visualizations	5	Pre=94 Recall=95 F1-Score=94.5
[85]	UCSD-AI4H	CT-Scan	349 COVID-19 Images, 397 Non-COVID-19 Images	GAN, Rescaling, Cropping	NA	DECAPS Architecture	Proposed Method	HAMs	Peekaboo Strategy	NA	Acc=87.6 Pre=84.3 Spe=85.2 F1-Score=87.1

Ref	Dataset Source	Modality	Dataset	Preprocessing	Framework	Model	Version	Classifier	Visualization	Fold	Results
[86]	Combination of Different Datasets	X-ray	99 COVID-19 Cases From the COVID19 Chest X-ray Dataset, 207 Images From Both Dataset	Balancing dataset, DA	Keras	GSA-DenseNet121-COVID-19	Modified Version	Softmax	NA	NA	Acc=98 Pre=98 F1-Score=98
[87]	COVID-Xray-5k Dataset	X-ray	536 COVID-19 Images, 5000 Non-COVID19	DA, Down Sampling	PyTorch	SqueezeNet	Standard Version	Softmax	NA	NA	Sen=97.5 Spec=97.8
[88]	Combination of Different Datasets	X-ray	207 COVID-19 Images, 5,863 Non-COVID-19 Images	DA	NA	DenseNet-161	Modified Version	Softmax	NA	NA	Acc=99 Pre=100 F1-Score=99
[89]	Combination of Different Datasets	X-ray	239 COVID-19 cases, 1,000 Bacterial or Viral Pneumonia Cases, 1,000 Healthy People	DA	Keras.	DCSL Framework	Modified Version	Softmax	T-SNE	5	Acc=97.01 Pre=97 Sen=97.09 F1-Score=96.98
[90]	Combination of Different Datasets	X-ray	108 COVID-19, 515 Other Pneumonia, 453 Normal	Class Balancing Methods, Binary Thresholding, Adaptive Total Variation Method	NA	NASNetLarge	Modified Version	Softmax	CAM and LIME Techniques	NA	Acc=98 Pre=88 Spe=95 F1-Score=89
[91]	Combination of Different Datasets	X-ray	225 COVID-19 Images, 108,948 Frontal View Images From 32,717 Unique Patients	DA	Keras with Tensor-Flow Backend	CN	12	FCMLP	Grad-CAM	5	Acc=95.3
[92]	Combination of Different Datasets	X-ray	180 COVID-19 Images, 6054 Pneumonia, 8851 Normal	NA	Keras	Concatenation of Xception and ResNet50V2	Modified Version	Softmax	NA	5	Acc=99.56
[93]	Combination of Different Datasets	X-ray	NA	Different Methods	PyTorch	COVID-DA	Modified Version	NA	Grad-CAM	NA	F1-Score=92.98 Pre=98.15 AUC=98.5
[94]	Combination of Different Datasets	X-ray	NA	Cropping, CLAHE Method, Resizing, DA	NA	CovIDNet	15	Softmax	NA	NA	Acc=98.4 Sen=100 Spe=96.97
[95]	Different Datasets	X-ray	Dataset_A (1579 Normal and 4429 Diseased), Dataset_B (4245 Pneumonia and 1763 Non-Pneumonia), Dataset_C (184 COVID-19 and 5824 Non-COVID19), Dataset_D (1579 Normal, 4245 Pneumonia, and 184 COVID-19)	DA, Oversampling	NA	3 ResNet18	Modified Version	Ensemble Models	NA	5	Acc=95.5 MCC=89.6 Pre=94 Recall=100 F1-Score=96.6
[96]	Clinical	CT-Scan	88 COVID-19 Patients, 100 Bacteria Pneumonia Patients, 86 Healthy Persons	Different Methods	OpenCV	DRE-Net (ResNet-50 Backbone)	Modified Version	Aggregation	Visualization	NA	Acc=94 AUC=99 Pre=96 F1-Score=94
[97]	Clinical	CT-Scan	1495 Patients of COVID-19 and 1027 Patients of Community Acquired Pneumonia (CAP)	Segmentation using VBNet, Feature Extraction	NA	AFS-DF	Proposed Architecture	Ensemble the Predicted Value	NA	5	Acc=91.79 Sen=93.05 Spe=89.95 AUC=96.35
[98]	Combination of Different Datasets	X-Ray, CT-Scan	200 of COVID-19, 200 Healthy, 200 Bacterial Pneumonia 200 Viral Pneumonia	NA	Caffe	ResNet101	Standard Version	Softmax	NA	10	Acc=98.75 Spe=97.50 Sen=100 Pre=96.43
[99]	Cohens GitHub	X-ray, CT-Scan	4 ARDS, 101 COVID-19, 2 No finding, 2 Pneumocystis-Pneumonia, 11 SARS, 6 Streptococcus	DA, Different Features, Feature Merging, Data Over-Sampling using SMOTE	NA	SAE (Feature Reduction)	6	SVM	NA	NA	Acc=71.92 Sen=68.91 Spe=93.91 Pre=69.89 F1-Score=69.13
[100]	Clinical	CT-Scan	44 COVID-19, 55 Typical Viral Pneumonia	ROIs Extraction Visual Inspection	NA	M-Inception	Modified Version	Combined Decision Tree and Adaboost	NA	NA	Acc=82.9 Sen=81 Spe=84 AUC=90 F1-Score=77
[101]	Combination of Different Datasets	X-ray	314 COVID-19	Segmentation using UNet, Standard Preprocessing, WeaklyLabeled DA	Keras with Tensor-Flow Backend	VGG16	Standard Version	Softmax	GradCAM	NA	Acc=99.26
[102]	Clinical	CT-Scan	109 COVID-19, 201 Non-COVID-19	Standard Preprocessing, Generating Pseudo-Infection Anomalies using BCDU-Net	NA	CovidCTNet	19	Softmax	NA	NA	Acc=90 Sen=83 Spe=92.85
[103]	Kaggle Data Repository	X-ray	150 COVID-19	Filtering, Segmentation using Thresholding	NA	CNN	11	Softmax	NA	NA	Acc=93
[52]	Combination of Different Datasets	CT-Scan	521 COVID-19, 521 Non-COVID-19	DA, Random Cropping Operation	NA	CNN with ShuffleNetV2 as the backbone	Standard Version	Linear Layer	NA	NA	Acc=91.21 Sen=90.52 Spe=91.58
[104]	COVIDx	X-ray	99 COVID-19, 18529 Non-COVID-19	DA	PyTorch	CoroNet (TFEN + CIN modules)	2 Independent FPAE + ResNet18	Softmax	Perturbation-based Algorithms for Generating Attribution Maps	NA	Acc=93.50 Sen=90 Pre=93.63 F1-Score=93.51
[105]	Different Datasets	CT-Scan	349 COVID-19, 397 Non-COVID-19	DA, Self-Trans Method	PyTorch	DenseNet-169	Standard Version	Softmax	Grad-CAM	NA	Acc=86 F1-Score=85 AUC=94
[106]	Clinical	CT-Scan	3389 COVID-19, 1593 Non-COVID-19	Standard Preprocessing, VB-Net Toolkit for Segmentation and Lung Mask Generation	PyTorch	3D ResNet34 Models with the Online Attention Module	Modified Version	Ensemble Learning	Grad-CAM	5	Acc=87.5 Sen=86.9 Spe=90.1 AUC=94.4 F1-Score=82.0
[107]	COVIDx	X-ray	238 COVID-19, 14896 Non-COVID-19	DA	TensorFlow	DenseNet-121	Modified Version	Softmax	Grad-CAM	10	Acc=96.4 Pre=96 Recall=96 F1-Score=96

Ref	Dataset	Modality	Number of Images	Preprocessing	Framework	Model	Version	Classifier	Visualization	K	Results
[108]	Clinical	CT-Scan	146 COVID-19, 149 Non-COVID-19	DA	PyTorch	DenseNet	Standard Version	Softmax	CAM	NA	Acc=92 Sen=97 Spe=87 F1-Score=93
[109]	Combination of Different Datasets	X-ray	158 COVID-19, 158 Non-COVID-19	NA	MATLAB	ResNet50	Standard Version	SVM	NA	NA	Acc=95.38 Sen=97.29 Spe=93.47
[110]	Clinical	CT-Scan	219 COVID-19, 399 Non-COVID-19	Preprocessing Based on HU Values	NA	ResNet18	29	Noisy-or Bayesian Function	NA	NA	Acc=86.7 Pre=81.3 F1-Score=83.9
[111]	Combination of Different Datasets	X-ray	455 COVID-19 Images, 2109 Non-COVID-19 Images	Rescaling, DA	Keras with Tensor-Flow Backend	MobileNet V2	Modified Version	NA	NA	10	Acc=99.18 Sen=97.36 Spe=99.42
[112]	Combination of Different Datasets	X-ray	403 COVID-19 Images, 721 Non-COVID-19 Images	Resizing, Normalizing, DA using CovidGAN Based AC-GAN	Keras	VGG16	Standard Version	Softmax	PCA Visualization	NA	Acc=95 Sen=90 Spe=97
[113]	Combination of Different Datasets	X-ray, CT-scan	6087 images (2780 Bacterial Pneumonia, 1724 Coronavirus (1493 Viral Pneumonia, 231 Covid19), 1583 Normal)	Intensity Normalization, CLAHE Method, DA, Resizing	Keras with Tensor-Flow Backend	Inception_ResNetV2	Standard Version	MLP	NA	5	Acc=92.18 Sen=92.11 Spec=96.06 Pre=92.38 F1-Score=92.07
[114]	Combination of Different Datasets	X-ray	69 COVID-19 Images, 79 Normal, 79 Pneumonia Bacterial, 79 Pneumonia Viruses	DA using GAN	MATLAB	GoogLeNet	Standard Version	Softmax	NA	NA	Acc=100 Pre=100 F1-Score=100
[115]	Combination of Different Datasets	CT-Scan	1118 COVID-19 Images, 96 Pneumonia Images, 107 Healthy Images	Different Methods	MATLAB	CNN (Feature Extraction)	12	LSTM	NA	NA	Acc=99.68
[116]	Combination of Different Datasets	X-ray	135 chest X-rays of COVID-19 and 320 Chest X-rays of Viral and Bacterial Pneumonia Unseen Data Consisting of 33 COVID-19 Data Cases, and 218 Pneumonia Cases	DA	NA	Resnet50, VGG16, Small CNN	Modified Version	Snapshot Ensemble of 21 Models	NA	10	Acc=91.24 AUC=94
[117]	Combination of Different Datasets	X-ray	224 Covid-19 cases, 504 Healthy Cases, 400 Bacteria, 314 Viral Pneumonia	Resizing	NA	MobileNet	Modified Version	NA	NA	NA	Acc=96.78 Sen=98.66 Spe=96.46
[118]	Combination of Different Datasets	X-ray	219 COVID-19, 1341 Normal Lung Images, 1345 Viral Pneumonia Images	Manually editing, Reshaping, DA	PyTorch	CheXNet (DenseNet121 Backbone)	Modified Version	Sigmoid	Heatmaps Generation using LRP	NA	Acc=98.3 Pre=98.3 F1-score=98.3
[119]	Different Datasets	X-ray	49 COVID-19 Images, 88,079 Non-COVID-19 Images	Standard Preprocessing	TorchXRayVision Library	DenseNet	Modified Version	Sigmoid, LR	t-SNE, Saliency Maps	NA	MAE=1.14
[120]	Combination of Different Datasets	X-ray	190 COVID-19, 1345 Viral Pneumonia, and 1341 Normal Chest X-ray Images	Resizing, Normalization, DA	MATLAB	SqueezeNet	Modified Version	Softmax	NA	5	Acc=98.3 Sen=96.7 Spe=100 Pre=100
[121]	COVID-CT-Dataset	CT-Scan	345 COVID-19, 397 Non COVID-19	Resizing, DA using CGAN, Normalizing	TensorFlow	ResNet50	Modified Version	Softmax	NA	NA	Acc=82.91 Sen=80.85 Spe=91.43
[122]	Combination of Different Datasets	X-ray	180 COVID-19 cases, 6054 Pneumonia Cases, 8851 Normal Cases	DA	Keras	Concatenation of the Xception and ResNet50V2	Modified Version	Softmax	NA	5	Acc=91.4
[123]	Kaggle	X-ray	70 COVID-19 and 80 Normal Images	Resizing, DA	NA	VGG16, VGG19	Modified Version	Softmax	NA	NA	Acc=97 Sen=100 Spe=94
[124]	Combination of Different Datasets	X-ray	215 COVID-19, 6045 CAP, 8851 Normal Images	DA	PyTorch	Different PreTrain Deep Networks	Modified Version	Softmax	NA	NA	Ensemble of Models: Acc=89.4 F1-Score=64
[125]	Combination of Different Datasets	X-ray	69 COVID-19, 79 Normal, 79 Pneumonia Bacterial, 79 Pneumonia Virus Images	Resizing, Neutrosophic Image Domain Conversion, Normalizing	MATLAB	GoogLeNet	Standard Version	Softmax	NA	NA	Acc=73.12
[126]	Combination of Different Datasets	X-ray, CT-scan	117 X-ray and 20 CT Scan of COVID-19, 117 Healthy X-ray Images, 20 Healthy CT Scan Images	Resizing, Normalizing	Keras with Tensor-Flow Backend	DenseNet121	Standard Version	Bagging Tree	Web-Based Application	10	Acc=99 Pre=96 F1-Score=96
[127]	Combination of Different Datasets	X-ray	181 COVID-19 Images, 364 Healthy Images	Normalizing, Resizing	NA	VGG-19	Modified Version	Softmax	NA	NA	Acc=96.3
[128]	Clinical	CT-Scan	151 COVID-19 Patient, 498 Non-COVID-19 Patient	Resizing, Padding, DA	NA	3D-CNN	15	Softmax	Visual Interpretation by Two Experienced Radiologists	NA	AUC=70
[129]	Public Datasets & Private Datasets	CT-Scan	1,684 COVID-19 Patient, 1,055 Pneumonia, 914 Normal Patients	Resizing	NA	Inception V1	Modified Version	Softmax	Interpretation by 6 Radiologists, t-SNE Method	10	Acc=95.78 AUC=99.4
[130]	Combination of Different Datasets	CT-Scan	413 COVID-19 Images and 439 Normal or Pneumonia Infected Patients Images	ResNet50 (Feature Extraction)	NA	CNN	14	Softmax	NA	10	Acc=93.01 Spe=94.77 Sen=91.45 Pre=95.18
[131]	Combination of Different Datasets	X-ray	142 COVID-19 Images, 142 Normal Images	Resizing, DA	NA	NCOVnet (VGG-16)	Modified Version	Softmax	NA	NA	Acc=97.62 Sen=97.62 Spe=78.57
[132]	Combination of Different Datasets	X-ray	326 COVID_19 Images, 984 Non-COVID-19 Images	Manual Annotation, Data Balancing and Augmentation Strategies, Normalizing, Resizing	NA	CNN with YOLO Predictor	54	Tensor of Prediction (ToP)	NA	5	Acc=97.40 Spe=99.056 Sen=85.15
[133]	Combination of Different Datasets	X-ray	250 COVID-19, 2,753 Other Pulmonary Diseases, 3,520 Healthy Images	Resizing, DA	NA	VGG-16	Modified Version	Softmax	Grad-CAM	NA	Acc=97 Sen=87 Spe=94

Work	Dataset	Modalities	Number of Cases	Preprocessing	DNN toolbox	DNN	Number of Layers	Classifier	Post Processing	K-Fold	Performance Criteria (%)
[134]	Combination of Different Datasets	X-ray	179 COVID-19, 179 Pneumonia, 179 Normal Images	Create a Noisy Snapshot Dataset	PyTorch	DenseNet-121, ShuffleNetV2, MobileNetV2	Modified/ Standard Versions	NA	t-SNE, GRAD-CAM	NA	Acc=84.3 AUROC=94
[135]	Another Reference	CT-Scan	73 Patients with COVID-19	MODE Algorithm for Hyper-Parameter Tuning	MATLAB	CNN	7	NA	NA	20	Acc=92 F1-Score=90 Sen=90 Spe=90
[136]	Clinical (3 Datasets)	X-ray	1583 Normal, 1493 Non-COVID Viral Pneumonia, 2780 Bacterial Pneumonia Images; 305 COVID_19 Images; 305 COVID-19,305 Normal, 305 Viral, 305 Bacterial Pneumonia Images	Reshaping to Different Resolutions, Normalizing	NA	Stacked Multi-Resolution CovXNet	Different Number of Layers	Stacking using Meta-Learner	Grad-CAM	5	Acc=97.4 Spe=94.7 F1-score=97.1 Recall=97.8 Pre=96.3 AUC=96.9
[137]	Clinical	CT-Scan	98 COVID-19 Patients, 103 Non-COVID-19 Patients	Visual Inspection	Google Colaboratory	BigBiGAN	NA	Linear Classifier	NA	NA	AUC=97.2 Sen=92 Spe=91
[138]	Combination of Different Datasets	X-ray	162 COVID-19 Images, 2003 Healthy, 4280 Viral and Bacterial Pneumonia, 400 Tuberculosis	Resizing, Normalizing	NA	Truncated InceptionNet V3	Modified Version	Softmax	Activation Maps Generation	10	Acc=98.77 Sen=95 Spe=99 Pre=99 F1-score=97
[139]	UCSD-AI4H Datasets	CT-Scan	349 Patients with Confirmed COVID and 397 Healthy Subjects	Resizing, Normalizing	Keras with Tensor-Flow Backed	DenseNet121	Standard Version	Nu-SVM	Web based CAD Implementation with Flask RESTful	10	Acc=90.61 Recall=90.80 Pre=89.76 F1-Score=90.13
[140]	Different Datasets	X-ray	219 COVID-19, 1341 Normal, 1345 Viral Pneumonia Images	Resizing, Normalizing, DA	PyTorch, Keras with Tensor-Flow Backend	DenseNet-201	Modified Version	Sigmoid	LRP	NA	Acc=99.4 Pre=99.5 F1-Score=99.4
[141]	Different Datasets	X-ray	536 COVID-19 Images, 619 Viral Pneumonia, and 668 Normal Images	White Balance Algorithm, CLAHE, Normalizing, Resizing	Keras with Tensor-Flow Backend	COVIDLite	38	Softmax	t-SNE,S Maps, Grad-CAM, LIME	5	Binary Acc=99.58 Multi-Class Acc=96.43
[142]	Combination of Different Datasets	X-ray	236 COVID-19 Images, 500 Healthy, 250 Viral Pneumonia, 250 Bacterial Pneumonia Images	Resizing, Zero-Padding, Percentile Cropping, Intensity Normalization	PyTorch	DenseNet161	Standard Version	Sigmoid	Occlusion, Saliency, Input X Gradient, Guided Backpropagation, Integrated Gradients, DeepLIFT	5	Pre=86.4 Recall=84.5 F1-score=85.4
[143]	Combination of Different Datasets	X-ray	X-rays of 327 Patients	Resizing, DA, Normalizing	NA	VGG16	Modified Version	Softmax	NA	5	Acc=84.1
[144]	COVIDx	X-ray	183 COVID-19 Images, 5551 Pneumonia Images, 8066 Normal Images	NA	NA	COVIDNet-CXR Small and COVID-Net-CXR Large	Standard Version	NA	UAPs using FGSM	NA	Acc=92.6 Avg Acc=94.4
[145]	Combination of Different Datasets	X-ray	127 COVID-19 Images, 127 Pneumonia Images, 127 Healthy Images	NA	MATLAB	ResNet50	Standard Version	SVM	NA	NA	Acc=95.33 Sen=95.33 F1-Score=95.34
[146]	Combination of Different Datasets	X-ray	738 Images of COVID-19, 5000 Normal, 4600 Images of CAP	DA, Normalization, Resizing, CLAHE, BEASF	NA	CNN	8	NA	Grad-CAM, LIME	NA	Acc=98.68 AUC=99.84 F1-Score=94
[147]	Clinical	CT-Scan	79 Patients with COVID-19, 100 Patients with Common Pneumonia, 130 People without Pneumonia.	DA	PyTorch	AD3D-MIL	Proposed Method	Bernouli Distribution	CAM	5	Acc=97.9 AUC=99 F1-Score=97.9 Pre=97.9 Recall=97.9

TABLE IV: Summary of DL segmentation methods used for COVID-19 detection.

Work	Dataset	Modalities	Number of Cases	Preprocessing	DNN toolbox	DNN	Number of Layers	Classifier	Post Processing	K-Fold	Performance Criteria (%)
[148]	Different Clinical Datasets	CT-Scan	157 International Patients	Detect and Measure Nodules, Lung Crop using U-net, DA	NA	ResNet50	Standard	Corona Score Computation	Grad-Cam, 3D Visualization	NA	AUC=99.6 Sen=98.2 Spe=92.2
[149]	Clinical	CT-Scan	549 COVID-19 Patients	HITL Strategy	NA	VB-Net	8 Block	NA	Quantitative Metrics Measurements	NA	DSC=91.6 Mean POI Estimation Error=0.3
[150]	Combination of Different Datasets	CT-Scan	610 COVID-19 Images, 695 Non-COVID-19 Images	Resizing, DA	PyTorch	DenseNet-169 + ASPP Layer	Standard	NA	NA	NA	F1-score=84.6 AUC=94.8 Acc=83
[151]	Combination of Different Datasets	X-ray and CT-Scan	1,341 Normal Samples, 3,875 Pneumonia Samples, 420 CT-Scan samples where 247 Normal Samples, 178 COVID-19 Samples; 704 Chest X-ray Images with Corresponding Masks, 267 CT-Scan Samples with Corresponding Masks	Resizing, DA, NABLA-3 Network for ROI Detection	TensorFlow	IRRCNN Model	7	Softmax	NA	NA	X-ray: Acc=84.67 CT: Acc=98.78
[152]	Different Datasets	CT-Scan	110 Axial CT-Scan Images From 60 Patients	Resizing, Grey Scaling (GL), DA	NA	Residual Attention U-Net	9 ResNeXt blocks+14 Layers	Sigmoid	Visualization	10	Acc=89 Pre=95 DSC=94
[153]	Different Datasets	CT-Scan	Different Number of Cases	Lung Segmentation using U-net with a VGG-16 Based Encoder, DA	NA	ResNet50	Standard	Sigmoid	GradCam, Combine the Fine Grain Maps to Create 3D Localization Maps, K-Means	NA	AUC=99.4 Sen=94 Spec=98

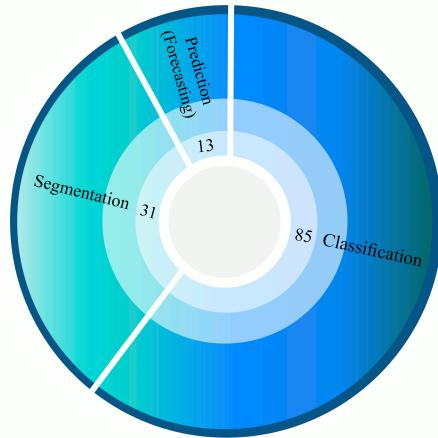| Ref	Dataset	Modality	Number of Cases	Preprocessing	Framework	Model	Structure	Output	Visualization	Folds	Results
[154]	COVID-CS Dataset	CT-Scan	144,167 CT-Scan Images of 400 COVID-19 Patients and 350 Uninfected Cases	DA, Segmentation using Encoder-Decoder Model	NA	Res2Net	Standard	Softmax	Visualization of Activation Mapping	NA	Avg Sen=95 Spe=93 Dice Score=78.3
[155]	Italian Society of Medical and Interventional Radiology	CT-Scan	473 CT Slices for COVID-19	Resizing, GL, Intensity Normalization	Keras	U-Net	50	Sigmoid	Visualization	NA	Dice Score=83.1 Sen=86.7 Spe=99.3
[156]	6 Different Datasets	X-ray	Different Number of Cases	Histogram, Segmentation using U-Net, Intensity Normalization	PyTorch	ResNet18	Standard	Softmax	t-SNE Clustering	NA	Acc=100 Sen=100 Spec=100 F1-score=100
[157]	COPD Dataset (Pretrain) / COVID-19 Set	CT-Scan	5000 COPDGene, Subjects / 470 COVID-19 Subjects	Standard Preprocessing	PyTorch	RTSU-Net	2 RU-Net	Sigmoid, Softmax	Different Methods	NA	IOU=92.2 ASSD=86.6
[158]	Different Dataset	X-ray	180 Images of 118 COVID-19 Subjects, 191 Normal, 54 Bacterial Pneumonia, 57 Tuberculosis, 20 Viral Pneumonia	Standard Preprocessing, Segmentation using FC-DenseNet103	PyTorch	ResNet18	Standard	Majority Voting	Probabilical Grad-CAM Saliency Map Visualization	NA	Sen=100 Pre=76.9
[159]	TCIA Dataset (Pretrain) / COVID-19 Clinical Dataset	CT-Scan	60 3D CT-Scan Lung / 150 3D Volumetric Chest CT Exams of COVID-19, CAP and NP Patients	DA, Fixed-Sized Sliding Window, Segmentation using U-Net	TensorFlow	CNN	27	Softmax	Multi-Window Voting Post-Processing Procedure and a Sequential Information Attention Module, CAM, Categorical-Specific Joint Saliency	5	Acc=96.2 Pre=97.3 Sen=94.5 Spe=95.3 AUC=97
[160]	COVID-19 Dataset	CT-Scan	60 Patients with COVID-19	Resizing, DA	PyTorch	MiniSeg	Proposed Structure	Sigmoid and Softmax	NA	NA	Sen=83.62 Spe=97.42 DSC=77.28 HD=68.07
[161]	Combination of Different Dataset	X-ray	313 COVID-19 Images, 7595 Normal, 6012 Pneumonia of Unknown Type, 2780 Bacterial Pneumonia Images	Segmentation using U-Net, Standard Preprocessing	NA	VGG-16, VGG-19, Inception-V3	Modified Version	Weighted Average Ensemble Method	Grad-CAM	NA	Acc=99.01 Sen=99.01 Pre=99.01 AUC=99.72
[162]	COVID-SemiSeg	CT-Scan	100 Labeled Images, 1600 Unlabeled Images of COVID-19	Pseudo Label Generation	PyTorch	Semi-Supervised Inf-Net+Multi-Class Segmentation	Modified Res2Net+ U-Net as Backbones	Sigmoid	NA	NA	Dice=54.1 Sen=56.4 Spe=96.7 MAE=5.7
[163]	Dataset I / Dataset II	X-ray	466 Normal, 860 Bacteria, 433 Viruses / 210 COVID-19, 330 Others	Adaptive Histogram, CLAHE Method, MoEx, Use U-Net to Segment Lung Area (VGG19), DA	NA	Cascade-SEMENet	Modified Version	Sigmoid	Grad-CAM	NA	Acc=85.6 F1-Score=86 / Acc=97.1 F1-Score=97
[58]	Clinical	CT-Scan	21,658 Images From 861 COVID-19 Patients	Cropping	Pytorch	COVID-SegNet	11 Blocks	Softmax	NA	NA	DSC=72.6 Sen=75.1 Pre=72.6
[164]	Clinical	CT-Scan	10 Axial Volumetric CT-Scans of COVID-19 Pneumonia Patients	Under-Sampling of the Majority Class	Keras with Tensor-Flow Backend	FCN-8s	NA	NA	NA	NA	Acc=100 F1-Score=90 Pre=98
[165]	Combination of Different Dataset	CT-Scan	449 COVID-19 Patients, 100 Normal, 98 Lung Cancer, 397 Other Pathology	Resizing, Intensity Normalization	Keras with Tensor-Flow Backend	Encoder and Two Decoders (2D U-NET Architecture) and MLP	24, 24, 15	Sigmoid	NA	NA	Acc=86 Sen=94 Spe=79 AUC=93 DSC=78.5
[166]	Clinical	CT-Scan	313 COVID-19, 229 Non-COVID-19	Normalizing, Resampling, DA, 3D Lung Mask Generation using 2D U-Net	PyTorch	DeCoVNet	20	Softmax	NA	NA	Acc=90.8
[167]	Clinical	CT-Scan	877 COVID-19, 991 Non-COVID-19	Visual Data Annotation and Quality, Normalization, 3D U-Net++ for Segmentation, DA	PyTorch	ResNet50	Standard Version	Softmax	NA	NA	Sen=97.4 Spe=92.2 AUC=99.1
[168]	Clinical	CT-Scan	1315 COVID-19 Scans, 3342 Non-COVID-19 Scans	Lobe Segmentation using 3D-Unet, Cropping, Resizing, DA	Keras with Tensor-Flow Backend	3D-ResNets with Prior-Attention Mechanism	Modified Version	Softmax	Heatmap Visualization	5	Acc=93.3 Sen=87.6 Spe=95.5
[169]	Clinical	LUS Images	17 COVID-19 Patients, 4 Were COVID-19 Suspected, and 14 Were Healthy	Labelling Process, DA, Reg-STN Model	NA	CNN	NA	Loss Function	Segmentation	5	NA
[170]	Clinical	CT-Scan	296 COVID-19 Images, 1735 CAP, 1325 Non-Pneumonia Images	Lung Segmentation using U-net	NA	COVNet	Modified Version	Softmax	Grad-CAM	NA	AUC=96 Sen=90 Spe=96
[171]	Clinical	CT-Scan	1266 COVID-19 Patients, 4106 Patients with Lung Cancer (Auxiliary Training Set)	DenseNet121-FPN for Lung Segmentation, 3-Dimensional Bounding Box, Non-Lung Area Suppression Operation	Keras	COVID-19Net	4 Dense Blocks +9 Layers	Sigmoid	Combined Feature Vectors, Multivariate Cox Proportional Hazard Model, Visualizations	NA	Acc=81.24 AUC=0.90 Sen=78.93 Spe=89.93 F1-Score=86.92
[172]	Clinical	CT-scan	219 From 110 Patients with COVID-19, 224 CT-Scan from patients, 175 CT-Scan From Healthy People	Segmentation using VNET-IR-RPN, DA	NA	ResNet-18 with Location-Attention Mechanism	Modified Version	Voting Strategy	Total Infection Confidence Score Calculation using Probability Formula of the Noisy-or Bayesian Function	NA	Acc=86.7
[173]	Clinical	CT-Scan	129 COVID-19 images	Segmentation Using U-Net, Different Preprocessing Methods	NA	ResNet18	Modified Version	Softmax	Calculate the Proportion of Infected Regions in Lung	NA	Acc=93.8 AUC=91.3 m-Dice=74.3
[174]	Clinical	CT-Scan	100 COVID-19 and 100 healthy controls	IDRL Landmarks, DI2IN Segmentation, Alignment, Resampling	Pytorch	DenseUNet	Modified Version	Softmax	Visualization	NA	Different Parameters
[175]	Clinical	CT-Scan	558 COVID-19 Patients	2D CNNs for the Segmentation	PyTorch	Student COPLE-Net+ EMA for Adaptive teacher+ Teacher COPLE-Net	Proposed Architecture	NA	Proposed Loss Function	NA	Dice=80.72 RVE=15.96
[176]	Combination of Different Datasets	CT-Scan	33 COVID-19 Patients, 32 Healthy Patients, 36 Patients with Other Lung Pathologies	Rescaling, Intensity Normalization, Creating Feature Map using U-Net	NA	Different Architectures	NA	NA	NA	3	AUC=95.1 Spearman Correlation=98

Fig. 20: Total number of investigations conducted in the field of classification, segmentation, and prediction of COVID-19 patients using DL techniques.
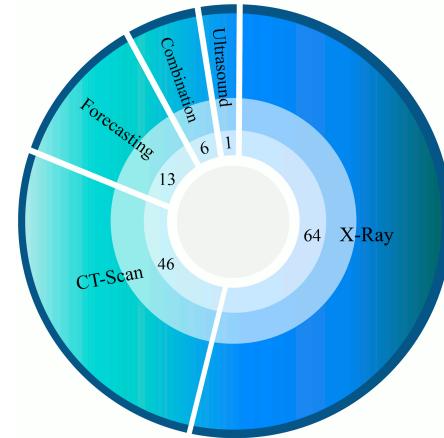

Fig. 21: Number of datasets used for COVID-19 detection and prediction based on the published papers using DL methods.

V. DISCUSSION

The main focus of this work is to select the best DL models employed to detect, segment the lungs, and predict the COVID-19 patients using DL techniques. The summary of works done on classification, segmentation, and prediction are presented in Tables III, IV, and V, respectively. Figure 20 depicts the total number of investigations conducted in the field of classification, segmentation, and prediction of COVID-19 using DL models. It can be noted from the figure that most works have been done on the detection of COVID-19 patients, and the least works are done on the forecasting due to shortage of available public databases.

The X-ray and CT images have been used to develop classification and segmentation DL models. Figure 21 shows the total number of times each modality is used in reviewed studies. It can be observed that most of the researchers have used X-ray images. This may be due to cheaper registration fees, and the fact that slice selection is not needed. Also, very few researches have used combined modalities of X-ray and CT images due to the absence of such a comprehensive database.

Various DL models developed for the automated detection of COVID-19 patients is shown in Figure 22. It can be noted from the figure that; different types of convolutional networks have been commonly used. Also, for the automated segmentation of lungs, various types of U-Net are more common.

Nowadays, a variety of toolboxes have been used to implement DL models. The number of toolboxes used for automated detection of COVID-19 by researches is shown in Figure 23. It can be noted that Keras toolbox is the most widely used for automated detection of COVID-19 patients; this is due to its simplicity and also availability of pre-trained models in this library, which are widely used by researchers.

The last part of this study is devoted to the classification algorithms developed using DL architectures. The softmax is most employed for automated detection of COVID-19 patients (Tables III to V). Figure 24 shows the number of
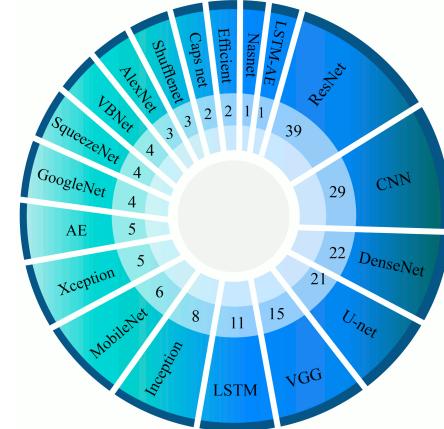

Fig. 22: Number of DL architectures used for COVID-19 detection and prediction based on published papers.

various classification algorithms used for automated detection of COVID-19 patients using DL techniques.

VI. CHALLENGES

With the rapid growth and spread of COVID-19 globally, researchers have confronted many serious challenges in designing and implementing CADS to diagnose and predict the disease. The most significant challenges associated with COVID-19 are data availability, DL networks architecture fixing, and hardware resources. Lack of availability of a huge public database comprising X-ray and CT images is the first challenge. Due to the limited number of patient data, many researchers have used pre-trained networks such as GoogLeNet and AlexNet. Nevertheless, the number of studies conducted on forecasting is limited as it requires a vast database.

One of the problems of employing pre-trained networks is that these models are often trained on the ImageNet database, which is entirely different from medical images. Hence, implementing efficient CADS to accurately and swiftly diagnose COVID-19 from X-Ray or CT images is still a challenging work. Physicians are not just convinced with X-ray or CT-scan images of patients to accurately diagnose COVID-19; they

TABLE V: Summary of DL models developed for the forecasting spread of COVID-19.

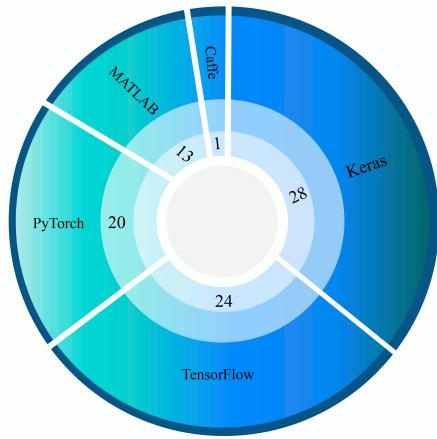| Work	Dataset	Preprocessing	DNN Toolbox	DNN	Number of layers	K-Fold	Post Processing	Performance Criteria
[177]	Johns Hopkins University and Canadian Health Authority	WT, ADF test	NA	LSTM	3	NA	NA	RMSE=45.70 Acc=92.67%
[178]	Surging News Network (a Media Outlet) and WHO	Reshaping	NA	CNN	7	NA	NA	MAE=102.943 RMSE=109.439
[179]	Google Trends Website	NA	Keras with TensorFlow Backend	LSTM	3	10	NA	RMSE=27.187
[180]	India Government	NA	MATLAB	LSTM	NA	NA	NA	Curves
[181]	Times Series Dataset of COVID-19 Confirmed Cases for Tunisia and China	Grid Search Technique, Sliding Window (SW)	NA	Stacked Ensemble Meta-Learners	DNN: 5 LSTM:5 CNN: 7	NA	Augmented Prediction	Acc=99% RMSE=2,396
[182]	Cumulative and New Confirmed Cases of Covid-19 in All of China and 31 Provinces/Cities in Mainland and Three Other Regions (Hong Kong, Macau and Taiwan)	Windowing, Normalizing	NA	Modified Auto-Encoders (MAE)	3	5	k-Means	Curves
[183]	COVID-19 Confirmed Data from Iran Ministry of Health and Medical Education, IRNA, ISNA Sources in Provincial Level and National Level	NA	TensorFlow	LSTM	NA	NA	NA	Curves
[184]	Combined of Local Trend Data and Weather Data	Feature Selection using OLS Regression, Network Hyper-Parameters Search	NA	LSTM	3	NA	Fuzzy Rule-Based Risk Categorization	RMSE=2300.8 Acc=78% Curves
[185]	WHO and Johns Hopkins University Datasets	Normalizing	NA	LSTM	4	NA	RMSLE	Curves
[186]	Johns Hopkins University, Lockdown dates of Countries Datasets	Windowing, Normalization, Proposed Improved Method	NA	LSTM	4	NA	NA	Curves
[187]	John Hopkins University, Oxford COVID-19 Government Response Tracker	Feature Selection, Spatially Weighted Adjacency Matrix Computation, Reshaping to 3D Tensor	NA	Variational LSTM-Autoencoder with Self-Attention Mechanism	3 Blocks	NA	NA	Curves
[188]	TheMinistry of Health and Family Welfare (Government of India)	Linear Weighted Moving Average Technique	Keras with TensorFlow Backend	Bi-LSTM	3	NA	NA	MAPE Less Than 3%

Fig. 23: Number of DL tools used for COVID-19 detection and prediction based on the published papers.
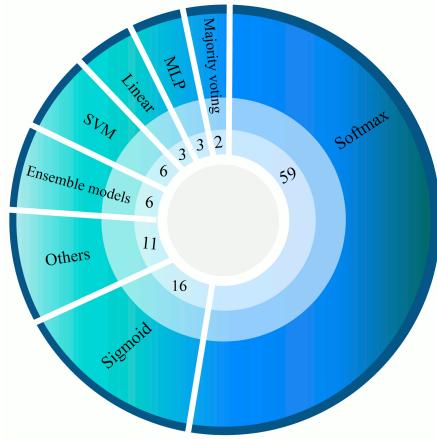

Fig. 24: Illustration of number of various classifier algorithms used in DL networks for automated detection of COVID-19 patients.

may use both modalities simultaneously. However, complete and comprehensive databases of the X-ray and CT-scan hybrid modalities for CADS research and implementation have not been provided for researchers' in the machine learning scope. For this reason, researchers combine different X-ray and CT-Scan datasets from various datasets, which may disrupt network training. Yielding the combined X-Ray and CT-Scan datasets pave the path to help quickly identify COVID-19 alongside DL networks. The third challenge in the data section is the non-reporting of phenotypic information, such as age and gender. The utilization of this information can amend and enhance the performance of DL algorithms.

Table IV summarizes the DL-based segmentation algorithms aimed at identifying areas suspected of corona in the X-ray and CT-scan images. One of the obstacles with databases is the absence of manual or ground truths for COVID-19 image segmentation areas. Therefore, many researchers have delineated these areas with the help of radiologists and trained the models such as U-Net, which is time-consuming. Consequently, the presence of dedicated databases of segmented images will help to get the best performing model. Also, it becomes easy to compare the performances with other authors who have worked on the same images.

In order to predict the prevalence of corona using DL methods, the nature of the COVID-19 is still relatively unknown, and the probability of mutation is a big issue. Therefore, to predict the prevalence of the disease, many factors like the average age of the society, policies to impede the spread of the disease by countries, climatic conditions, and infection of neighbor/friend/family member.

Lack of access to appropriate hardware resources is another challenge. Implementing DL architectures in CADS for corona diagnosis demands strong hardware resources, which unfortunately is not ordinarily accessible for many researchers. Although tools such as Google Colab have partially obviated this problem, employing these tools in real medical applications is still challenging. For this reason, in most studies, researchers have not provided practical CADS systems such as web or Windows software to detect COVID-19.

VII. Conclusion and Future Works

COVID-19 is an emerging pandemic disease that, in a short period of time, can severely endanger the health of many people throughout the world. It directly affects the lung cells, and if not accurately diagnosed early, can cause irreversible damage, including death. The disease is accurately detected by the specialists using X-ray or CT images together with PCR

results. The PCR results indicate the type of lung disease, such as pulmonary tuberculosis, instead of COVID-19. In this study, a comprehensive review of the accomplished studies of COVID-19 diagnosis was carried out using DL networks. The public databases available to diagnose and predict COVID-19 are presented. The state-of-art DL techniques employed for the diagnosis, segmentation, and forecasting of the spread of COVID-19 are presented in Tables III, IV, V, respectively. One of the challenges to develop a robust and accurate COVID 19 diagnosis system is the availability of an extensive public database. We strongly feel that, with more public databases, better DL models can be developed by researchers to detect and predict the COVID19 accurately. Hence, this will help to develop the best performing model. We feel that data fusion models can help to improve the performance of diagnosis and prediction. The features extracted from the ML and DL models can be fused to develop an accurate model.

Also, developing the accurate segmentation model is challenging as it involves delineating the lungs by the experts. Having an accurate ground truth is another challenge.

APPENDIX A
EVALUATION METRICS

This section discusses the evaluation metrics used in different studies. In these metrics, True positive (TP) is the correct classification ratio of the positive class, False positive (FP) is the incorrect prediction ratio of the positives, True negative (TN) is the correct classification ratio of the negative class, and finally False negative (FN) is the incorrect prediction ratio of the negatives [189].

A. Receiver Operating Characteristic Curve (ROC-Curve)

The receiver operating characteristic curve (ROC-curve) illustrates the performance of the proposed model at all classification thresholds. It is the graph of true positive rate vs. false positive rate (TPR vs. FPR).

$$TPR = \frac{TP}{TP + FN} \tag{1}$$

$$FPR = \frac{FP}{FP + TN} \tag{2}$$

B. Area under the ROC Curve (AUC)

AUC depicts the area under the ROC-curve incorporated from (0, 0) to (1, 1). It presents the cumulative measure of all possible classification thresholds. AUC has a range from 0 to 1. A 100% wrong classification will have AUC value 0.0, while a 100% correct classified version will have the AUC value 1.0. It has two folded benefits; first, it is scale-invariant, meaning that entailed value shows how well the model is predicted rather than examining the absolute values. The second benefit is that it is classification-threshold invariant, as it will validate the models performance irrespective of the threshold being chosen.

C. Accuracy

Accuracy verifies that how many samples are correctly classified.

$$Accuracy(Acc) = \frac{TP + TN}{TP + TN + FP + FN} \tag{3}$$

D. Specificity

It is the rate of recognition of negative samples correctly.

$$Specificity(Spe) = \frac{TN}{TN + FP} \tag{4}$$

E. Sensitivity

It is the rate of recognition of positive samples correctly.

$$Sensitivity(Sen) = \frac{TP}{TP + FN} \tag{5}$$

F. Precision

It calculates how precise the model performs by examining the correct true positives from the predicted ones.

$$Precision(Pre) = \frac{TP}{TP + FP} \tag{6}$$

G. F1-Score

F1-score is the function of sensitivity and precision, which tries to find a balance between sensitivity and precision.

$$F1 - Score = 2 * \frac{Pre * Sen}{Pre + Sen} \tag{7}$$

H. Average Accuracy

It is a measure of effectiveness of the classification technique.

$$Avg_{Acc} = \frac{\sum^{n} \frac{TP+TN}{TP+TN+FP+FN}}{n} \tag{8}$$

where n is the total number of outputs of the system.

I. Jaccard Index

It is a measure of similarity rate between two sample groups.

$$Jac_{idx} = \frac{TP}{TP + FP + FN} \tag{9}$$

J. Dice-Coefficient

It is a statistical measure of similarity rate between two sample groups.

$$Dice_{cof} = \frac{2 * TP}{2 * TP + FP + FN} \tag{10}$$

References

[1] J. F.-W. Chan, S. Yuan, K.-H. Kok, K. K.-W. To, H. Chu, J. Yang, F. Xing, J. Liu, C. C.-Y. Yip, R. W.-S. Poon *et al.*, "A familial cluster of pneumonia associated with the 2019 novel coronavirus indicating person-to-person transmission: a study of a family cluster," *The Lancet*, vol. 395, no. 10223, pp. 514–523, 2020.

[2] X. Peng, X. Xu, Y. Li, L. Cheng, X. Zhou, and B. Ren, "Transmission routes of 2019-ncov and controls in dental practice," *International Journal of Oral Science*, vol. 12, no. 1, pp. 1–6, 2020.

[3] S. Tian, W. Hu, L. Niu, H. Liu, H. Xu, and S.-Y. Xiao, "Pulmonary pathology of early phase 2019 novel coronavirus (covid-19) pneumonia in two patients with lung cancer," *Journal of Thoracic Oncology*, 2020.

[4] T. C. Lan, M. F. Allan, L. Malsick, S. Khandwala, S. S. Nyeo, M. Bathe, A. Griffiths, and S. Rouskin, "Structure of the full sars-cov-2 rna genome in infected cells," *bioRxiv*, 2020.

[5] M. S. Razai, K. Doerholt, S. Ladhani, and P. Oakeshott, "Coronavirus disease 2019 (covid-19): a guide for uk gps," *BMJ*, vol. 368, 2020.

[6] A. Remuzzi and G. Remuzzi, "Covid-19 and italy: what next?" *The Lancet*, 2020.

[7] C. Sohrabi, Z. Alsafi, N. ONeill, M. Khan, A. Kerwan, A. Al-Jabir, C. Iosifidis, and R. Agha, "World health organization declares global emergency: A review of the 2019 novel coronavirus (covid-19)," *International Journal of Surgery*, 2020.

[8] A. E. Hassanien, L. N. Mahdy, K. A. Ezzat, H. H. Elmousalami, and H. A. Ella, "Automatic x-ray covid-19 lung image classification system based on multi-level thresholding and support vector machine," *medRxiv*, 2020.

[9] S. Kadry, V. Rajinikanth, S. Rho, N. S. M. Raja, V. S. Rao, and K. P. Thanaraj, "Development of a machine-learning system to classify lung ct scan images into normal/covid-19 class," *arXiv preprint arXiv:2004.13122*, 2020.

[10] W. H. Self, D. M. Courtney, C. D. McNaughton, R. G. Wunderink, and J. A. Kline, "High discordance of chest x-ray and computed tomography for detection of pulmonary opacities in ed patients: implications for diagnosing pneumonia," *The American journal of emergency medicine*, vol. 31, no. 2, pp. 401–405, 2013.

[11] G. D. Rubin, C. J. Ryerson, L. B. Haramati, N. Sverzellati, J. P. Kanne, S. Raoof, N. W. Schluger, A. Volpi, J.-J. Yim, I. B. Martin *et al.*, "The role of chest imaging in patient management during the covid-19 pandemic: a multinational consensus statement from the fleischner society," *Chest*, 2020.

[12] L. Orioli, M. P. Hermans, J.-P. Thissen, D. Maiter, B. Vandeleene, and J.-C. Yombi, "Covid-19 in diabetic patients: related risks and specifics of management," in *Annales D'endocrinologie*. Elsevier, 2020.

[13] "https://www.ecdc.europa.eu/en/geographical-distribution-2019-ncov-cases," https://www.ecdc.europa.eu/en/geographical-distribution-2019-ncov-cases, 2020.

[14] R. Alizadehsani, M. Behjati, Z. Roshanzamir, S. Hussain, N. Abedini, F. Hasanzadeh, A. Khosravi, A. Shoeibi, M. Roshanzamir, P. Moradnejad *et al.*, "Risk factors prediction, clinical outcomes, and mortality of covid-19 patients," *medRxiv*, 2020.

[15] L. J. Kroft, L. van der Velden, I. H. Girón, J. J. Roelofs, A. de Roos, and J. Geleijns, "Added value of ultra–low-dose computed tomography, dose equivalent to chest x-ray radiography, for diagnosing chest pathology," *Journal of thoracic imaging*, vol. 34, no. 3, p. 179, 2019.

[16] N. Ghassemi, A. Shoeibi, and M. Rouhani, "Deep neural network with generative adversarial networks pre-training for brain tumor classification based on mr images," *Biomedical Signal Processing and Control*, vol. 57, p. 101678, 2020.

[17] M. Talo, O. Yildirim, U. B. Baloglu, G. Aydin, and U. R. Acharya, "Convolutional neural networks for multi-class brain disease detection using mri images," *Computerized Medical Imaging and Graphics*, vol. 78, p. 101673, 2019.

[18] N. Ghassemi, A. Shoeibi, M. Rouhani, and H. Hosseini-Nejad, "Epileptic seizures detection in eeg signals using tqwt and ensemble learning," in *2019 9th International Conference on Computer and Knowledge Engineering (ICCKE)*. IEEE, 2019, pp. 403–408.

[19] U. R. Acharya, S. L. Oh, Y. Hagiwara, J. H. Tan, and H. Adeli, "Deep convolutional neural network for the automated detection and diagnosis of seizure using eeg signals," *Computers in biology and medicine*, vol. 100, pp. 270–278, 2018.

[20] M. Mohammadpoor, A. Shoeibi, H. Zare, and H. Shojaee, "A hierarchical classification method for breast tumor detection," *Iranian Journal of Medical Physics*, vol. 13, no. 4, pp. 261–268, 2016.

[21] D. Arefan, A. A. Mohamed, W. A. Berg, M. L. Zuley, J. H. Sumkin, and S. Wu, "Deep learning modeling using normal mammograms for predicting breast cancer risk," *Medical physics*, vol. 47, no. 1, pp. 110–118, 2020.

[22] A. Z. Khuzani, M. Heidari, and S. A. Shariati, "Covid-classifier: An automated machine learning model to assist in the diagnosis of covid-19 infection in chest x-ray images," *medRxiv*, 2020.

[23] X. Mei, H.-C. Lee, K.-y. Diao, M. Huang, B. Lin, C. Liu, Z. Xie, Y. Ma, P. M. Robson, M. Chung *et al.*, "Artificial intelligence–enabled rapid diagnosis of patients with covid-19," *Nature Medicine*, pp. 1–5, 2020.

[24] A. Esteva, B. Kuprel, R. A. Novoa, J. Ko, S. M. Swetter, H. M. Blau, and S. Thrun, "Dermatologist-level classification of skin cancer with deep neural networks," *nature*, vol. 542, no. 7639, pp. 115–118, 2017.

[25] M. A. Mazurowski, M. Buda, A. Saha, and M. R. Bashir, "Deep learning in radiology: An overview of the concepts and a survey of the state of the art with focus on mri," *Journal of magnetic resonance imaging*, vol. 49, no. 4, pp. 939–954, 2019.

[26] T. M. Tuan, T. T. Ngan, C. N. Giap *et al.*, "Semisupervised fuzzy clustering methods for x-ray image segmentation," in *Handbook of Data Science Approaches for Biomedical Engineering*. Elsevier, 2020, pp. 251–289.

[27] A. Shoeibi, N. Ghassemi, H. Hosseini-Nejad, and M. Rouhani, "An efficient brain mr images segmentation hardware using kernel fuzzy c-means," in *2019 26th National and 4th International Iranian Conference on Biomedical Engineering (ICBME)*. IEEE, 2019, pp. 93–99.

[28] O. Ronneberger, P. Fischer, and T. Brox, "U-net: Convolutional networks for biomedical image segmentation," in *International Conference on Medical image computing and computer-assisted intervention*. Springer, 2015, pp. 234–241.

[29] J. P. Cohen, P. Morrison, L. Dao, K. Roth, T. Q. Duong, and M. Ghassemi, "Covid-19 image data collection: Prospective predictions are the future," *arXiv 2006.11988*, 2020. [Online]. Available: https://github.com/ieee8023/covid-chestxray-dataset

[30] J. Zhao, Y. Zhang, X. He, and P. Xie, "Covid-ct-dataset: a ct scan dataset about covid-19," *arXiv preprint arXiv:2003.13865*, 2020.

[31] J. Born, G. Brändle, M. Cossio, M. Disdier, J. Goulet, J. Roulin, and N. Wiedemann, "Pocovid-net: Automatic detection of covid-19 from a new lung ultrasound imaging dataset (pocus)," *arXiv preprint arXiv:2004.12084*, 2020.

[32] J. M. Banda, R. Tekumalla, G. Wang, J. Yu, T. Liu, Y. Ding, and G. Chowell, "A large-scale covid-19 twitter chatter dataset for open scientific research–an international collaboration," *arXiv preprint arXiv:2004.03688*, 2020.

[33] R. Hu, G. Ruan, S. Xiang, M. Huang, Q. Liang, and J. Li, "Automated diagnosis of covid-19 using deep learning and data augmentation on chest ct," *medRxiv*, 2020.

[34] Z. Q. L. Linda Wang and A. Wong, "Covid-net: A tailored deep convolutional neural network design for detection of covid-19 cases from chest radiography images," 2020.

[35] L. Zhang, M. Wang, M. Liu, and D. Zhang, "A survey on deep learning for neuroimaging-based brain disorder analysis," *arXiv preprint arXiv:2005.04573*, 2020.

[36] M. Z. Alom, T. M. Taha, C. Yakopcic, S. Westberg, P. Sidike, M. S. Nasrin, B. C. Van Esesn, A. A. S. Awwal, and V. K. Asari, "The history began from alexnet: A comprehensive survey on deep learning approaches," *arXiv preprint arXiv:1803.01164*, 2018.

[37] A. Krizhevsky, I. Sutskever, and G. E. Hinton, "Imagenet classification with deep convolutional neural networks," in *Advances in neural information processing systems*, 2012, pp. 1097–1105.

[38] K. Simonyan and A. Zisserman, "Very deep convolutional networks for large-scale image recognition," *arXiv preprint arXiv:1409.1556*, 2014.

[39] C. Szegedy, W. Liu, Y. Jia, P. Sermanet, S. Reed, D. Anguelov, D. Erhan, V. Vanhoucke, and A. Rabinovich, "Going deeper with convolutions," in *Proceedings of the IEEE conference on computer vision and pattern recognition*, 2015, pp. 1–9.

[40] K. He, X. Zhang, S. Ren, and J. Sun, "Identity mappings in deep residual networks," in *European conference on computer vision*. Springer, 2016, pp. 630–645.

[41] C. Szegedy, S. Ioffe, V. Vanhoucke, and A. A. Alemi, "Inception-v4, inception-resnet and the impact of residual connections on learning," in *Thirty-first AAAI conference on artificial intelligence*, 2017.

[42] M. Karim, T. Döhmen, D. Rebholz-Schuhmann, S. Decker, M. Cochez, O. Beyan *et al.*, "Deepcovidexplainer: Explainable covid-19 predictions based on chest x-ray images," *arXiv preprint arXiv:2004.04582*, 2020.

[43] G. Huang, Z. Liu, L. Van Der Maaten, and K. Q. Weinberger, "Densely connected convolutional networks," in *Proceedings of the*

IEEE conference on computer vision and pattern recognition, 2017, pp. 4700–4708.

[44] F. Chollet, "Xception: Deep learning with depthwise separable convolutions," in *Proceedings of the IEEE conference on computer vision and pattern recognition*, 2017, pp. 1251–1258.

[45] A. G. Howard, M. Zhu, B. Chen, D. Kalenichenko, W. Wang, T. Weyand, M. Andreetto, and H. Adam, "Mobilenets: Efficient convolutional neural networks for mobile vision applications," *arXiv preprint arXiv:1704.04861*, 2017.

[46] M. Sandler, A. Howard, M. Zhu, A. Zhmoginov, and L.-C. Chen, "Mobilenetv2: Inverted residuals and linear bottlenecks," in *Proceedings of the IEEE conference on computer vision and pattern recognition*, 2018, pp. 4510–4520.

[47] F. N. Iandola, S. Han, M. W. Moskewicz, K. Ashraf, W. J. Dally, and K. Keutzer, "Squeezenet: Alexnet-level accuracy with 50x fewer parameters and¡ 0.5 mb model size," *arXiv preprint arXiv:1602.07360*, 2016.

[48] S. Sabour, N. Frosst, and G. E. Hinton, "Dynamic routing between capsules," in *Advances in neural information processing systems*, 2017, pp. 3856–3866.

[49] B. Zoph, V. Vasudevan, J. Shlens, and Q. V. Le, "Learning transferable architectures for scalable image recognition," in *Proceedings of the IEEE conference on computer vision and pattern recognition*, 2018, pp. 8697–8710.

[50] X. Zhang, X. Zhou, M. Lin, and J. Sun, "Shufflenet: An extremely efficient convolutional neural network for mobile devices," in *Proceedings of the IEEE conference on computer vision and pattern recognition*, 2018, pp. 6848–6856.

[51] N. Ma, X. Zhang, H.-T. Zheng, and J. Sun, "Shufflenet v2: Practical guidelines for efficient cnn architecture design," in *Proceedings of the European conference on computer vision (ECCV)*, 2018, pp. 116–131.

[52] R. Hu, G. Ruan, S. Xiang, M. Huang, Q. Liang, and J. Li, "Automated diagnosis of covid-19 using deep learning and data augmentation on chest ct," *medRxiv*, 2020.

[53] M. Tan and Q. V. Le, "Efficientnet: Rethinking model scaling for convolutional neural networks," *arXiv preprint arXiv:1905.11946*, 2019.

[54] X. Yi, E. Walia, and P. Babyn, "Generative adversarial network in medical imaging: A review," *Medical image analysis*, vol. 58, p. 101552, 2019.

[55] I. Goodfellow, J. Pouget-Abadie, M. Mirza, B. Xu, D. Warde-Farley, S. Ozair, A. Courville, and Y. Bengio, "Generative adversarial nets," in *Advances in neural information processing systems*, 2014, pp. 2672–2680.

[56] J. Long, E. Shelhamer, and T. Darrell, "Fully convolutional networks for semantic segmentation," in *Proceedings of the IEEE conference on computer vision and pattern recognition*, 2015, pp. 3431–3440.

[57] V. Badrinarayanan, A. Kendall, and R. Cipolla, "Segnet: A deep convolutional encoder-decoder architecture for image segmentation," *IEEE transactions on pattern analysis and machine intelligence*, vol. 39, no. 12, pp. 2481–2495, 2017.

[58] Q. Yan, B. Wang, D. Gong, C. Luo, W. Zhao, J. Shen, Q. Shi, S. Jin, L. Zhang, and Z. You, "Covid-19 chest ct image segmentation–a deep convolutional neural network solution," *arXiv preprint arXiv:2004.10987*, 2020.

[59] O. Ronneberger, P. Fischer, and T. Brox, "U-net: Convolutional networks for biomedical image segmentation," in *International Conference on Medical image computing and computer-assisted intervention*. Springer, 2015, pp. 234–241.

[60] T. Zhou, S. Canu, and S. Ruan, "An automatic covid-19 ct segmentation network using spatial and channel attention mechanism." *arXiv preprint arXiv:2004.06673*, 2020.

[61] S. Gao, M.-M. Cheng, K. Zhao, X.-Y. Zhang, M.-H. Yang, and P. H. Torr, "Res2net: A new multi-scale backbone architecture," *IEEE transactions on pattern analysis and machine intelligence*, 2019.

[62] J. Chung, C. Gulcehre, K. Cho, and Y. Bengio, "Empirical evaluation of gated recurrent neural networks on sequence modeling," *arXiv preprint arXiv:1412.3555*, 2014.

[63] P. Baldi, "Autoencoders, unsupervised learning, and deep architectures," in *Proceedings of ICML workshop on unsupervised and transfer learning*, 2012, pp. 37–49.

[64] I. Tolstikhin, O. Bousquet, S. Gelly, and B. Schoelkopf, "Wasserstein auto-encoders," *arXiv preprint arXiv:1711.01558*, 2017.

[65] M. Farooq and A. Hafeez, "Covid-resnet: A deep learning framework for screening of covid19 from radiographs," *arXiv preprint arXiv:2003.14395*, 2020.

[66] A. Narin, C. Kaya, and Z. Pamuk, "Automatic detection of coronavirus disease (covid-19) using x-ray images and deep convolutional neural networks," *arXiv preprint arXiv:2003.10849*, 2020.

[67] H. S. Maghdid, A. T. Asaad, K. Z. Ghafoor, A. S. Sadiq, and M. K. Khan, "Diagnosing covid-19 pneumonia from x-ray and ct images using deep learning and transfer learning algorithms," *arXiv preprint arXiv:2004.00038*, 2020.

[68] E. E.-D. Hemdan, M. A. Shouman, and M. E. Karar, "Covidx-net: A framework of deep learning classifiers to diagnose covid-19 in x-ray images," *arXiv preprint arXiv:2003.11055*, 2020.

[69] J. Zhang, Y. Xie, Y. Li, C. Shen, and Y. Xia, "Covid-19 screening on chest x-ray images using deep learning based anomaly detection," *arXiv preprint arXiv:2003.12338*, 2020.

[70] L. Wang and A. Wong, "Covid-net: A tailored deep convolutional neural network design for detection of covid-19 cases from chest x-ray images," *arXiv preprint arXiv:2003.09871*, 2020.

[71] F. Ucar and D. Korkmaz, "Covidiagnosis-net: Deep bayes-squeezenet based diagnostic of the coronavirus disease 2019 (covid-19) from x-ray images," *Medical Hypotheses*, p. 109761, 2020.

[72] B. Ghoshal and A. Tucker, "Estimating uncertainty and interpretability in deep learning for coronavirus (covid-19) detection," *arXiv preprint arXiv:2003.10769*, 2020.

[73] M. Toğaçar, B. Ergen, and Z. Cömert, "Covid-19 detection using deep learning models to exploit social mimic optimization and structured chest x-ray images using fuzzy color and stacking approaches," *Computers in Biology and Medicine*, p. 103805, 2020.

[74] X. Wu, H. Hui, M. Niu, L. Li, L. Wang, B. He, X. Yang, L. Li, H. Li, J. Tian *et al.*, "Deep learning-based multi-view fusion model for screening 2019 novel coronavirus pneumonia: a multicentre study," *European Journal of Radiology*, p. 109041, 2020.

[75] T. Ozturk, M. Talo, E. A. Yildirim, U. B. Baloglu, O. Yildirim, and U. R. Acharya, "Automated detection of covid-19 cases using deep neural networks with x-ray images," *Computers in Biology and Medicine*, p. 103792, 2020.

[76] A. A. Ardakani, A. R. Kanafi, U. R. Acharya, N. Khadem, and A. Mohammadi, "Application of deep learning technique to manage covid-19 in routine clinical practice using ct images: Results of 10 convolutional neural networks," *Computers in Biology and Medicine*, p. 103795, 2020.

[77] A. Abbas, M. M. Abdelsamea, and M. M. Gaber, "Classification of covid-19 in chest x-ray images using detrac deep convolutional neural network," *arXiv preprint arXiv:2003.13815*, 2020.

[78] R. M. Pereira, D. Bertolini, L. O. Teixeira, C. N. Silla Jr, and Y. M. Costa, "Covid-19 identification in chest x-ray images on flat and hierarchical classification scenarios," *Computer Methods and Programs in Biomedicine*, p. 105532, 2020.

[79] N. E. M. Khalifa, M. H. N. Taha, A. E. Hassanien, and S. Elghamrawy, "Detection of coronavirus (covid-19) associated pneumonia based on generative adversarial networks and a fine-tuned deep transfer learning model using chest x-ray dataset," *arXiv preprint arXiv:2004.01184*, 2020.

[80] U. Ozkaya, S. Ozturk, and M. Barstugan, "Coronavirus (covid-19) classification using deep features fusion and ranking technique," *arXiv preprint arXiv:2004.03698*, 2020.

[81] P. Afshar, S. Heidarian, F. Naderkhani, A. Oikonomou, K. N. Plataniotis, and A. Mohammadi, "Covid-caps: A capsule network-based framework for identification of covid-19 cases from x-ray images," *arXiv preprint arXiv:2004.02696*, 2020.

[82] A. I. Khan, J. L. Shah, and M. M. Bhat, "Coronet: A deep neural network for detection and diagnosis of covid-19 from chest x-ray images," *Computer Methods and Programs in Biomedicine*, p. 105581, 2020.

[83] K. Hammoudi, H. Benhabiles, M. Melkemi, F. Dornaika, I. Arganda-Carreras, D. Collard, and A. Scherpereel, "Deep learning on chest x-ray images to detect and evaluate pneumonia cases at the era of covid-19," *arXiv preprint arXiv:2004.03399*, 2020.

[84] E. Luz, P. L. Silva, R. Silva, and G. Moreira, "Towards an efficient deep learning model for covid-19 patterns detection in x-ray images," *arXiv preprint arXiv:2004.05717*, 2020.

[85] A. Mobiny, P. A. Cicalese, S. Zare, P. Yuan, M. Abavisani, C. C. Wu, J. Ahuja, P. M. de Groot, and H. Van Nguyen, "Radiologist-level covid-19 detection using ct scans with detail-oriented capsule networks," *arXiv preprint arXiv:2004.07407*, 2020.

[86] D. Ezzat, H. A. Ella *et al.*, "Gsa-densenet121-covid-19: a hybrid deep learning architecture for the diagnosis of covid-19 disease based on gravitational search optimization algorithm," *arXiv preprint arXiv:2004.05084*, 2020.

[87] S. Minaee, R. Kafieh, M. Sonka, S. Yazdani, and G. J. Soufi, "Deep-covid: Predicting covid-19 from chest x-ray images using deep transfer learning," *arXiv preprint arXiv:2004.09363*, 2020.

[88] J. de Moura, L. Ramos, P. L. Vidal, M. Cruz, L. Abelairas, E. Castro, J. Novo, and M. Ortega, "Deep convolutional approaches for the analysis of covid-19 using chest x-ray images from portable devices," *medRxiv*, 2020.

[89] T. Li, Z. Han, B. Wei, Y. Zheng, Y. Hong, and J. Cong, "Robust screening of covid-19 from chest x-ray via discriminative cost-sensitive learning," *arXiv preprint arXiv:2004.12592*, 2020.

[90] N. S. Punn and S. Agarwal, "Automated diagnosis of covid-19 with limited posteroanterior chest x-ray images using fine-tuned deep neural networks," *arXiv preprint arXiv:2004.11676*, 2020.

[91] S. Basu and S. Mitra, "Deep learning for screening covid-19 using chest x-ray images," *arXiv preprint arXiv:2004.10507*, 2020.

[92] M. Rahimzadeh and A. Attar, "A new modified deep convolutional neural network for detecting covid-19 from x-ray images," *arXiv preprint arXiv:2004.08052*, 2020.

[93] Y. Zhang, S. Niu, Z. Qiu, Y. Wei, P. Zhao, J. Yao, J. Huang, Q. Wu, and M. Tan, "Covid-da: Deep domain adaptation from typical pneumonia to covid-19," *arXiv preprint arXiv:2005.01577*, 2020.

[94] M. Ramadhan, A. Faza, L. Lubis, R. Yunus, T. Salamah, D. Handayani, I. Lestariningsih, A. Resa, C. Alam, P. Prajitno *et al.*, "Fast and accurate detection of covid-19-related pneumonia from chest x-ray images with novel deep learning model," *arXiv preprint arXiv:2005.04562*, 2020.

[95] S. Misra, S. Jeon, S. Lee, R. Managuli, and C. Kim, "Multi-channel transfer learning of chest x-ray images for screening of covid-19," *arXiv preprint arXiv:2005.05576*, 2020.

[96] Y. Song, S. Zheng, L. Li, X. Zhang, X. Zhang, Z. Huang, J. Chen, H. Zhao, Y. Jie, R. Wang *et al.*, "Deep learning enables accurate diagnosis of novel coronavirus (covid-19) with ct images," *medRxiv*, 2020.

[97] L. Sun, Z. Mo, F. Yan, L. Xia, F. Shan, Z. Ding, W. Shao, F. Shi, H. Yuan, H. Jiang *et al.*, "Adaptive feature selection guided deep forest for covid-19 classification with chest ct," *arXiv preprint arXiv:2005.03264*, 2020.

[98] I. Razzak, S. Naz, A. Rehman, A. Khan, and A. Zaib, "Improving coronavirus (covid-19) diagnosis using deep transfer learning," *medRxiv*, 2020.

[99] S. Ozturk, U. Ozkaya, and M. Barstugan, "Classification of coronavirus images using shrunken features," *medRxiv*, 2020.

[100] S. Wang, B. Kang, J. Ma, X. Zeng, M. Xiao, J. Guo, M. Cai, J. Yang, Y. Li, X. Meng *et al.*, "A deep learning algorithm using ct images to screen for corona virus disease (covid-19)," *MedRxiv*, 2020.

[101] S. Rajaraman and S. Antani, "Training deep learning algorithms with weakly labeled pneumonia chest x-ray data for covid-19 detection," *medRxiv*, 2020.

[102] T. Javaheri, M. Homayounfar, Z. Amoozgar, R. Reiazi, F. Homay-ounieh, E. Abbas, A. Laali, A. R. Radmard, M. H. Gharib, S. A. J. Mousavi *et al.*, "Covidctnet: An open-source deep learning approach to identify covid-19 using ct image," *arXiv preprint arXiv:2005.03059*, 2020.

[103] M. Jamil, I. Hussain *et al.*, "Automatic detection of covid-19 infection from chest x-ray using deep learning," *medRxiv*, 2020.

[104] S. Khobahi, C. Agarwal, and M. Soltanalian, "Coronet: A deep network architecture for semi-supervised task-based identification of covid-19 from chest x-ray images," *medRxiv*, 2020.

[105] X. He, X. Yang, S. Zhang, J. Zhao, Y. Zhang, E. Xing, and P. Xie, "Sample-efficient deep learning for covid-19 diagnosis based on ct scans," *medRxiv*, 2020.

[106] X. Ouyang, J. Huo, L. Xia, F. Shan, J. Liu, Z. Mo, F. Yan, Z. Ding, Q. Yang, B. Song *et al.*, "Dual-sampling attention network for diagnosis of covid-19 from community acquired pneumonia," *IEEE Transactions on Medical Imaging*, 2020.

[107] L. Sarker, M. Islam, T. Hannan, and A. Zakaria, "Covid-densenet: A deep learning architecture to detect covid-19 from chest radiology images," *Preprints*, 2020.

[108] S. Yang, L. Jiang, Z. Cao, L. Wang, J. Cao, R. Feng, Z. Zhang, X. Xue, Y. Shi, and F. Shan, "Deep learning for detecting corona virus disease 2019 (covid-19) on high-resolution computed tomography: a pilot study," *Annals of Translational Medicine*, vol. 8, no. 7, 2020.

[109] P. K. Sethy and S. K. Behera, "Detection of coronavirus disease (covid-19) based on deep features," *Preprints*, vol. 2020030300, p. 2020, 2020.

[110] C. Butt, J. Gill, D. Chun, and B. A. Babu, "Deep learning system to screen coronavirus disease 2019 pneumonia," *Applied Intelligence*, p. 1, 2020.

[111] I. D. Apostolopoulos, S. I. Aznaouridis, and M. A. Tzani, "Extracting possibly representative covid-19 biomarkers from x-ray images with deep learning approach and image data related to pulmonary diseases," *Journal of Medical and Biological Engineering*, p. 1, 2020.

[112] A. Waheed, M. Goyal, D. Gupta, A. Khanna, F. Al-Turjman, and P. R. Pinheiro, "Covidgan: Data augmentation using auxiliary classifier gan for improved covid-19 detection," *IEEE Access*, vol. 8, pp. 91 916–91 923, 2020.

[113] K. Elasnaoui and Y. Chawki, "Using x-ray images and deep learning for automated detection of coronavirus disease," *Journal of Biomolecular Structure and Dynamics*, no. just-accepted, pp. 1–22, 2020.

[114] M. Loey, F. Smarandache, and N. E. M Khalifa, "Within the lack of chest covid-19 x-ray dataset: A novel detection model based on gan and deep transfer learning," *Symmetry*, vol. 12, no. 4, p. 651, 2020.

[115] A. M. Hasan, M. M. AL-Jawad, H. A. Jalab, H. Shaiba, R. W. Ibrahim, and A. R. AL-Shamasneh, "Classification of covid-19 coronavirus, pneumonia and healthy lungs in ct scans using q-deformed entropy and deep learning features," *Entropy*, vol. 22, no. 5, p. 517, 2020.

[116] L. O. Hall, R. Paul, D. B. Goldgof, and G. M. Goldgof, "Finding covid-19 from chest x-rays using deep learning on a small dataset," *arXiv preprint arXiv:2004.02060*, 2020.

[117] I. D. Apostolopoulos and T. A. Mpesiana, "Covid-19: automatic detection from x-ray images utilizing transfer learning with convolutional neural networks," *Physical and Engineering Sciences in Medicine*, p. 1, 2020.

[118] P. R. Bassi and R. Attux, "A deep convolutional neural network for covid-19 detection using chest x-rays," *arXiv preprint arXiv:2005.01578*, 2020.

[119] J. P. Cohen, L. Dao, P. Morrison, K. Roth, Y. Bengio, B. Shen, A. Abbasi, M. Hoshmand-Kochi, M. Ghassemi, H. Li *et al.*, "Predicting covid-19 pneumonia severity on chest x-ray with deep learning," *arXiv preprint arXiv:2005.11856*, 2020.

[120] M. E. Chowdhury, T. Rahman, A. Khandakar, R. Mazhar, M. A. Kadir, Z. B. Mahbub, K. R. Islam, M. S. Khan, A. Iqbal, N. Al-Emadi *et al.*, "Can ai help in screening viral and covid-19 pneumonia?" *arXiv preprint arXiv:2003.13145*, 2020.

[121] M. Loey, G. Manogaran, and N. E. M. Khalifa, "A deep transfer learning model with classical data augmentation and cgan to detect covid-19 from chest ct radiography digital images," 2020.

[122] M. Rahimzadeh and A. Attar, "A modified deep convolutional neural network for detecting covid-19 and pneumonia from chest x-ray images based on the concatenation of xception and resnet50v2," *Informatics in Medicine Unlocked*, p. 100360, 2020.

[123] N. Bansal and S. Sridhar, "Classification of x-ray images for detecting covid-19 using deep transfer learning," 2020.

[124] B. D. Goodwin, C. Jaskolski, C. Zhong, and H. Asmani, "Intra-model variability in covid-19 classification using chest x-ray images," *arXiv preprint arXiv:2005.02167*, 2020.

[125] N. E. M. Khalifa, F. Smarandache, and M. Loey, "A study of the neutrosophic set significance on deep transfer learning models: An experimental case on a limited covid-19 chest x-ray dataset," *Preprints*, 2020.

[126] S. H. Kassani, P. H. Kassasni, M. J. Wesolowski, K. A. Schneider, and R. Deters, "Automatic detection of coronavirus disease (covid-19) in x-ray and ct images: A machine learning-based approach," *arXiv preprint arXiv:2004.10641*, 2020.

[127] S. Vaid, R. Kalantar, and M. Bhandari, "Deep learning covid-19 detection bias: accuracy through artificial intelligence," *International Orthopaedics*, p. 1, 2020.

[128] J. Pu, J. Leader, A. Bandos, J. Shi, P. Du, J. Yu, B. Yang, S. Ke, Y. Guo, J. B. Field *et al.*, "Any unique image biomarkers associated with covid-19?" *European Radiology*, p. 1, 2020.

[129] K. Yang, X. Liu, Y. Yang, X. Liao, R. Wang, X. Zeng, Y. Wang, M. Zhang, and T. Zhang, "End-to-end covid-19 screening with 3d deep learning on chest computed tomography," 2020.

[130] Y. Pathak, P. K. Shukla, A. Tiwari, S. Stalin, S. Singh, and P. K. Shukla, "Deep transfer learning based classification model for covid-19 disease," *IRBM*, 2020.

[131] H. Panwar, P. Gupta, M. K. Siddiqui, R. Morales-Menendez, and V. Singh, "Application of deep learning for fast detection of covid-19 in x-rays using ncovnet," *Chaos, Solitons & Fractals*, p. 109944, 2020.

[132] M. A. Al-antari, C.-H. Hua, and S. Lee, "Fast deep learning computer-aided diagnosis against the novel covid-19 pandemic from digital chest x-ray images," 2020.

[133] L. Brunese, F. Mercaldo, A. Reginelli, and A. Santone, "Explainable deep learning for pulmonary disease and coronavirus covid-19 detection from x-rays," *Computer Methods and Programs in Biomedicine*, p. 105608, 2020.

[134] X. Li, C. Li, and D. Zhu, "Covid-mobilexpert: On-device covid-19 screening using snapshots of chest x-ray," *arXiv preprint arXiv:2004.03042*, 2020.

[135] D. Singh, V. Kumar, and M. Kaur, "Classification of covid-19 patients from chest ct images using multi-objective differential evolution–based convolutional neural networks," *European Journal of Clinical Microbiology & Infectious Diseases*, pp. 1–11, 2020.

[136] T. Mahmud, M. A. Rahman, and S. A. Fattah, "Covxnet: A multi-dilation convolutional neural network for automatic covid-19 and other pneumonia detection from chest x-ray images with transferable multi-receptive feature optimization," *Computers in Biology and Medicine*, p. 103869, 2020.

[137] J. Song, H. Wang, Y. Liu, W. Wu, G. Dai, Z. Wu, P. Zhu, W. Zhang, K. W. Yeom, and K. Deng, "End-to-end automatic differentiation of the coronavirus disease 2019 (covid-19) from viral pneumonia based on chest ct," *European journal of nuclear medicine and molecular imaging*, pp. 1–9, 2020.

[138] D. Das, K. Santosh, and U. Pal, "Truncated inception net: Covid-19 outbreak screening using chest x-rays," *Physical and engineering sciences in medicine*, pp. 1–11, 2020.

[139] A. Saeedi, M. Saeedi, and A. Maghsoudi, "A novel and reliable deep learning web-based tool to detect covid-19 infection form chest ct-scan," *arXiv preprint arXiv:2006.14419*, 2020.

[140] P. R. Bassi and R. Attux, "A deep convolutional neural network for covid-19 detection using chest x-rays," *arXiv preprint arXiv:2005.01578*, 2020.

[141] M. Siddhartha and A. Santra, "Covidlite: A depth-wise separable deep neural network with white balance and clahe for detection of covid-19," *arXiv preprint arXiv:2006.13873*, 2020.

[142] S. Chatterjee, F. Saad, C. Sarasaen, S. Ghosh, R. Khatun, P. Radeva, G. Rose, S. Stober, O. Speck, and A. Nürnberger, "Exploration of interpretability techniques for deep covid-19 classification using chest x-ray images," *arXiv preprint arXiv:2006.02570*, 2020.

[143] P. G. Moutounet-Cartan, "Deep convolutional neural networks to diagnose covid-19 and other pneumonia diseases from posteroanterior chest x-rays," *arXiv preprint arXiv:2005.00845*, 2020.

[144] H. Hirano, K. Koga, and K. Takemoto, "Vulnerability of deep neural networks for detecting covid-19 cases from chest x-ray images to universal adversarial attacks," *arXiv preprint arXiv:2005.11061*, 2020.

[145] P. K. Sethy, S. K. Behera, P. K. Ratha, and P. Biswas, "Detection of coronavirus disease (covid-19) based on deep features and support vector machine."

[146] A. Haghanifar, M. M. Majdabadi, and S. Ko, "Covid-cxnet: Detecting covid-19 in frontal chest x-ray images using deep learning," *arXiv preprint arXiv:2006.13807*, 2020.

[147] G. Wang, X. Liu, C. Li, Z. Xu, J. Ruan, H. Zhu, T. Meng, K. Li, N. Huang, and S. Zhang, "A noise-robust framework for automatic segmentation of covid-19 pneumonia lesions from ct images," *IEEE Transactions on Medical Imaging*, 2020.

[148] O. Gozes, M. Frid-Adar, H. Greenspan, P. D. Browning, H. Zhang, W. Ji, A. Bernheim, and E. Siegel, "Rapid ai development cycle for the coronavirus (covid-19) pandemic: Initial results for automated detection & patient monitoring using deep learning ct image analysis," *arXiv preprint arXiv:2003.05037*, 2020.

[149] F. Shan, Y. Gao, J. Wang, W. Shi, N. Shi, M. Han, Z. Xue, and Y. Shi, "Lung infection quantification of covid-19 in ct images with deep learning," *arXiv preprint arXiv:2003.04655*, 2020.

[150] J. Zhao, Y. Zhang, X. He, and P. Xie, "Covid-ct-dataset: a ct scan dataset about covid-19," *arXiv preprint arXiv:2003.13865*, 2020.

[151] M. Z. Alom, M. Rahman, M. S. Nasrin, T. M. Taha, and V. K. Asari, "Covid_mtnet: Covid-19 detection with multi-task deep learning approaches," *arXiv preprint arXiv:2004.03747*, 2020.

[152] X. Chen, L. Yao, and Y. Zhang, "Residual attention u-net for automated multi-class segmentation of covid-19 chest ct images," *arXiv preprint arXiv:2004.05645*, 2020.

[153] O. Gozes, M. Frid-Adar, N. Sagie, H. Zhang, W. Ji, and H. Greenspan, "Coronavirus detection and analysis on chest ct with deep learning," *arXiv preprint arXiv:2004.02640*, 2020.

[154] Y.-H. Wu, S.-H. Gao, J. Mei, J. Xu, D.-P. Fan, C.-W. Zhao, and M.-M. Cheng, "Jcs: An explainable covid-19 diagnosis system by joint classification and segmentation," *arXiv preprint arXiv:2004.07054*, 2020.

[155] T. Zhou, S. Canu, and S. Ruan, "An automatic covid-19 ct segmentation based on u-net with attention mechanism," *arXiv preprint arXiv:2004.06673*, 2020.

[156] E. Tartaglione, C. A. Barbano, C. Berzovini, M. Calandri, and M. Grangetto, "Unveiling covid-19 from chest x-ray with deep learning: a hurdles race with small data," *arXiv preprint arXiv:2004.05405*, 2020.

[157] W. Xie, C. Jacobs, J.-P. Charbonnier, and B. van Ginneken, "Relational modeling for robust and efficient pulmonary lobe segmentation in ct scans," *IEEE Transactions on Medical Imaging*, 2020.

[158] Y. Oh, S. Park, and J. C. Ye, "Deep learning covid-19 features on cxr using limited training data sets," *IEEE Transactions on Medical Imaging*, 2020.

[159] S. Hu, Y. Gao, Z. Niu, Y. Jiang, L. Li, X. Xiao, M. Wang, E. F. Fang, W. Menpes-Smith, J. Xia *et al.*, "Weakly supervised deep learning for covid-19 infection detection and classification from ct images," *IEEE Access*, 2020.

[160] Y. Qiu, Y. Liu, and J. Xu, "Miniseg: An extremely minimum network for efficient covid-19 segmentation," *arXiv preprint arXiv:2004.09750*, 2020.

[161] S. Rajaraman, J. Siegelman, P. O. Alderson, L. S. Folio, L. R. Folio, and S. K. Antani, "Iteratively pruned deep learning ensembles for covid-19 detection in chest x-rays," *arXiv preprint arXiv:2004.08379*, 2020.

[162] D.-P. Fan, T. Zhou, G.-P. Ji, Y. Zhou, G. Chen, H. Fu, J. Shen, and L. Shao, "Inf-net: Automatic covid-19 lung infection segmentation from ct images," *IEEE Transactions on Medical Imaging*, 2020.

[163] D. Lv, W. Qi, Y. Li, L. Sun, and Y. Wang, "A cascade network for detecting covid-19 using chest x-rays," *arXiv preprint arXiv:2005.01468*, 2020.

[164] A. Voulodimos, E. Protopapadakis, I. Katsamenis, A. Doulamis, and N. Doulamis, "Deep learning models for covid-19 infected area segmentation in ct images," *medRxiv*, 2020.

[165] A. Amyar, R. Modzelewski, and S. Ruan, "Multi-task deep learning based ct imaging analysis for covid-19: Classification and segmentation," *medRxiv*, 2020.

[166] C. Zheng, X. Deng, Q. Fu, Q. Zhou, J. Feng, H. Ma, W. Liu, and X. Wang, "Deep learning-based detection for covid-19 from chest ct using weak label," *medRxiv*, 2020.

[167] S. Jin, B. Wang, H. Xu, C. Luo, L. Wei, W. Zhao, X. Hou, W. Ma, Z. Xu, Z. Zheng *et al.*, "Ai-assisted ct imaging analysis for covid-19 screening: Building and deploying a medical ai system in four weeks," *medRxiv*, 2020.

[168] J. Wang, Y. Bao, Y. Wen, H. Lu, H. Luo, Y. Xiang, X. Li, C. Liu, and D. Qian, "Prior-attention residual learning for more discriminative covid-19 screening in ct images," *IEEE Transactions on Medical Imaging*, 2020.

[169] S. Roy, W. Menapace, S. Oei, B. Luijten, E. Fini, C. Saltori, I. Huijben, N. Chennakeshava, F. Mento, A. Sentelli *et al.*, "Deep learning for classification and localization of covid-19 markers in point-of-care lung ultrasound," *IEEE Transactions on Medical Imaging*, 2020.

[170] L. Li, L. Qin, Z. Xu, Y. Yin, X. Wang, B. Kong, J. Bai, Y. Lu, Z. Fang, Q. Song *et al.*, "Artificial intelligence distinguishes covid-19 from community acquired pneumonia on chest ct," *Radiology*, p. 200905, 2020.

[171] S. Wang, Y. Zha, W. Li, Q. Wu, X. Li, M. Niu, M. Wang, X. Qiu, H. Li, H. Yu *et al.*, "A fully automatic deep learning system for covid-19 diagnostic and prognostic analysis," *European Respiratory Journal*, 2020.

[172] C. Butt, J. Gill, D. Chun, and B. A. Babu, "Deep learning system to screen coronavirus disease 2019 pneumonia," *Applied Intelligence*, p. 1, 2020.

[173] W. Wu, Y. Shi, X. Li, Y. Zhou, P. Du, S. Lv, T. Liang, and J. Sheng, "Deep learning to estimate the physical proportion of infected region of lung for covid-19 pneumonia with ct image set," *arXiv preprint arXiv:2006.05018*, 2020.

[174] S. Chaganti, A. Balachandran, G. Chabin, S. Cohen, T. Flohr, B. Georgescu, P. Grenier, S. Grbic, S. Liu, F. Mellot *et al.*, "Quantification of tomographic patterns associated with covid-19 from chest ct," *arXiv preprint arXiv:2004.01279*, 2020.

[175] Z. Han, B. Wei, Y. Hong, T. Li, J. Cong, X. Zhu, H. Wei, and W. Zhang, "Accurate screening of covid-19 using attention based deep 3d multiple instance learning," *IEEE Transactions on Medical Imaging*, 2020.

[176] M. Goncharov, M. Pisov, A. Shevtsov, B. Shirokikh, A. Kurmukov, I. Blokhin, V. Chernina, A. Solovev, V. Gombolevskiy, S. Morozov *et al.*, "Ct-based covid-19 triage: Deep multitask learning improves joint identification and severity quantification," *arXiv preprint arXiv:2006.01441*, 2020.

[177] V. K. R. Chimmula and L. Zhang, "Time series forecasting of covid-19 transmission in canada using lstm networks," *Chaos, Solitons & Fractals*, p. 109864, 2020.

[178] C.-J. Huang and P.-H. Kuo, "Multiple-input deep convolutional neural network model for short-term photovoltaic power forecasting," *IEEE Access*, vol. 7, pp. 74 822–74 834, 2019.

[179] S. M. Ayyoubzadeh, S. M. Ayyoubzadeh, H. Zahedi, M. Ahmadi, and S. R. N. Kalhori, "Predicting covid-19 incidence through analysis of google trends data in iran: data mining and deep learning pilot study," *JMIR Public Health and Surveillance*, vol. 6, no. 2, p. e18828, 2020.

[180] A. Tomar and N. Gupta, "Prediction for the spread of covid-19 in india and effectiveness of preventive measures," *Science of The Total Environment*, p. 138762, 2020.

[181] N. B. Yahia, M. D. Kandara, and N. B. B. Saoud, "Deep ensemble learning method to forecast covid-19 outbreak," 2020.

[182] Z. Hu, Q. Ge, L. Jin, and M. Xiong, "Artificial intelligence forecasting of covid-19 in china," *arXiv preprint arXiv:2002.07112*, 2020.

[183] M. Azarafza, M. Azarafza, and J. Tanha, "Covid-19 infection forecasting based on deep learning in iran," *medRxiv*, 2020.

[184] R. Pal, A. A. Sekh, S. Kar, and D. K. Prasad, "Neural network based country wise risk prediction of covid-19," *arXiv preprint arXiv:2004.00959*, 2020.

[185] L. R. Kolozsvari, T. Berczes, A. Hajdu, R. Gesztelyi, A. TIba, I. Varga, G. J. Szollosi, S. Harsanyi, S. Garboczy, and J. Zsuga, "Predicting the epidemic curve of the coronavirus (sars-cov-2) disease (covid-19) using artificial intelligence," *medRxiv*, 2020.

[186] B. Yan, X. Tang, B. Liu, J. Wang, Y. Zhou, G. Zheng, Q. Zou, Y. Lu, and W. Tu, "An improved method of covid-19 case fitting and prediction based on lstm," *arXiv preprint arXiv:2005.03446*, 2020.

[187] M. R. Ibrahim, J. Haworth, A. Lipani, N. Aslam, T. Cheng, and N. Christie, "Variational-lstm autoencoder to forecast the spread of coronavirus across the globe," *medRxiv*, 2020.

[188] P. Arora, H. Kumar, and B. K. Panigrahi, "Prediction and analysis of covid-19 positive cases using deep learning models: A descriptive case study of india," *Chaos, Solitons & Fractals*, p. 110017, 2020.

[189] K. Munir, H. Elahi, A. Ayub, F. Frezza, and A. Rizzi, "Cancer diagnosis using deep learning: a bibliographic review," *Cancers*, vol. 11, no. 9, p. 1235, 2019.